Physical processes and biological productivity in the upwelling regions ofthe tropical Atlantic

Peter Brandt, Gael Alory, Founi Mesmin Awo, Marcus Dengler, Sandrine Djakoure, Rodrigue Anicet Imbol Koungue, Julien Jouanno, Mareike Koerner, Marisa Roch, Mathieu Rouault

Ocean Sci., 19, 581–601, 2023
https://doi.org/10.5194/os-19-581-2023

Ocean Science Open Access EGU

Physical processes and biological productivity in the upwelling regions of the tropical Atlantic

Peter Brandt[1,2], Gaël Alory[3], Founi Mesmin Awo[4], Marcus Dengler[1], Sandrine Djakouré[5], Rodrigue Anicet Imbol Koungue[1], Julien Jouanno[3], Mareike Körner[1], Marisa Roch[1], and Mathieu Rouault[4,†]

[1]GEOMAR Helmholtz Centre for Ocean Research Kiel, Kiel, Germany
[2]Faculty of Mathematics and Natural Sciences, Kiel University, Kiel, Germany
[3]LEGOS, CNES/CNRS/IRD/UPS, Toulouse, France
[4]Nansen-Tutu Centre for Marine Environmental Research, Department of Oceanography, University of Cape Town, Cape Town, South Africa
[5]LASMES, UFR SSMT, Felix Houphouët-Boigny University, Abidjan, Côte d'Ivoire
[†]deceased

Correspondence: Peter Brandt (pbrandt@geomar.de)

Received: 29 November 2022 – Discussion started: 5 December 2022
Revised: 11 April 2023 – Accepted: 16 April 2023 – Published: 11 May 2023

Abstract. In this paper, we review observational and modelling results on the upwelling in the tropical Atlantic between 10° N and 20° S. We focus on the physical processes that drive the seasonal variability of surface cooling and the upward nutrient flux required to explain the seasonality of biological productivity. We separately consider the equatorial upwelling system, the coastal upwelling system of the Gulf of Guinea and the tropical Angolan upwelling system. All three tropical Atlantic upwelling systems have in common a strong seasonal cycle, with peak biological productivity during boreal summer. However, the physical processes driving the upwelling vary between the three systems. For the equatorial regime, we discuss the wind forcing of upwelling velocity and turbulent mixing, as well as the underlying dynamics responsible for thermocline movements and current structure. The coastal upwelling system in the Gulf of Guinea is located along its northern boundary and is driven by both local and remote forcing. Particular emphasis is placed on the Guinea Current, its separation from the coast and the shape of the coastline. For the tropical Angolan upwelling, we show that this system is not driven by local winds but instead results from the combined effect of coastally trapped waves, surface heat and freshwater fluxes, and turbulent mixing. Finally, we review recent changes in the upwelling systems associated with climate variability and global warming and address possible responses of upwelling systems in future scenarios.

Dedication. In memory of our dear colleague and friend Prof. Mathieu Rouault whose passion for upwelling dynamics was limitless.

1 Introduction

The tropical oceans are important to the Earth system for several reasons. The ocean receives a large part of shortwave radiation from the sun arriving at the Earth's surface that must be redistributed horizontally and vertically. Similar important exchanges of carbon dioxide, oxygen and other trace gases occur at the interface between the tropical ocean and the overlying atmosphere. Tropical marine ecosystems are among the most productive ones, with high relevance for global fisheries (Longhurst, 1993). They are associated with a substantial carbon flux from the near-surface into the deep ocean (Kiko et al., 2017). At the same time, the tropical oceans are affected by modes of natural climate variability that have reverberations around the globe, including the Pacific El Niño or the Atlantic Niño. Climate warming and change are thought to profoundly affect the tropical oceans. On the one hand, they impact natural climate variability via an intensification of climate extremes or changes in natural variability (Cai et al., 2018; Crespo et al., 2022; Prigent et al., 2020b; Yang et al., 2022). On the other hand, they are thought to change the wind forcing of tropical oceans

(Wang et al., 2015; Bakun, 1990) or to enhance stratification, thereby impacting subduction, upwelling and air–sea gas exchange, with consequences for acidification, deoxygenation (Oschlies et al., 2018) and marine ecosystems.

The zonal extent of the tropical Atlantic is similar to that of the Indian Ocean and about 3 times smaller than that of the Pacific Ocean. The difference in size between the Pacific and Atlantic oceans seems to be the main reason for the dominance of interannual climate variability in the tropical Pacific, while the tropical Atlantic has the largest variability on seasonal timescales (Keenlyside and Latif, 2007; Burls et al., 2011). Moreover, the annual and semiannual cycles of primary production are strongly enhanced in the tropical Atlantic compared to in the tropical Pacific (Mao et al., 2020). A geographical peculiarity of the tropical Atlantic Ocean is the existence of the Gulf of Guinea which, in addition to its eastern boundary, boarders to the African continent in the north, approximately along 5° N from 10° W to 10° E. There are several major rivers flowing into the tropical Atlantic, including the Amazon, Congo and Niger rivers (Fig. 1).

Based on satellite data, Longhurst (1993) provided a first systematic overview of the different open-ocean and coastal upwelling systems in the tropical Atlantic. Today, mean satellite chlorophyll concentration (Fig. 1) reveals enhanced productivity in the different coastal upwelling regions of the tropical Atlantic, such as in the Gulf of Guinea upwelling system (GGUS – here defined as 8° W–3° E, 1° width coastal band) and in the tropical Angolan upwelling system (TAUS – here defined as 6–17° S, 1° width coastal band). The permanent northern Benguela upwelling system is located south of the TAUS, with the Kunene upwelling cell at about 17° S forming its northern boundary (Siegfried et al., 2019). The equatorial Atlantic upwelling system (EAUS – here defined as 3° N–3° S, 20° W–0° W) is an open-ocean upwelling region characterized by albeit an enhanced but, in comparison to the coastal upwelling systems, relatively weak chlorophyll concentration (note the logarithmic scale for the chlorophyll concentration in Fig. 1; Grodsky et al., 2008). Nevertheless, the EAUS is still of major importance for the overall biological productivity in the tropical Atlantic due to its large oceanic extent. Besides the tropical upwelling systems, enhanced chlorophyll concentration is found in the regions of the Amazon and the Congo river mouths. In the region of the Niger River mouth, no comparable signal of enhanced chlorophyll is found, likely due to the much-reduced discharge of the Niger compared to that of the Amazon or Congo rivers (Fig. 1).

The tropical Atlantic upwelling is an element of the shallow overturning circulation and the subtropical cells (STCs), and it is connected to the subduction in the eastern subtropics via equatorward thermocline flow and poleward Ekman transport in the surface layer (Schott et al., 2004; Fu et al., 2022; Tuchen et al., 2020). At the Equator, the Equatorial Undercurrent (EUC) transports thermocline waters eastward, toward the EAUS. Due to the presence of the Atlantic meridional overturning circulation, these waters are almost exclusively of southern-hemispheric origin (Schott et al., 1998; Johns et al., 2014; Tuchen et al., 2022a). Part of the waters recirculates into the westward current branches of the South Equatorial Current, the northern and the central South Equatorial Current, or contributes to supplying the southward flow along the eastern boundary within the Gabon–Congo Undercurrent and the Angola Current (Kolodziejczyk et al., 2014; Kopte et al., 2017). The GGUS is supplied by the Guinea Current and the Guinea Undercurrent. While the waters of the Guinea Current mostly originate in the North Equatorial Countercurrent, a similar connection between the North Equatorial Undercurrent and the Guinea Undercurrent is less obvious (Bourlès et al., 2002; Djakouré et al., 2017; Herbert et al., 2016). Due to the much smaller width of the Atlantic compared to the Pacific, the thermocline waters arriving from the western boundary in the eastern-basin upwelling systems are less enhanced in nitrate and less reduced in oxygen in the Atlantic compared to in the Pacific (Brandt et al., 2015; Chai et al., 1996; Radenac et al., 2020).

The tropical Atlantic and its upwelling systems undergo a strong seasonal cycle (Fig. 1b–d). The main drivers are the seasonally varying winds associated with the meridional migration of the intertropical convergence zone (ITCZ; Fig. 2). During boreal summer, the ITCZ migrates northward, resulting in strongly enhanced upwelling-favouring easterly winds along the Equator and the establishment of the Atlantic cold tongue (ACT) centred around 10° W (Fig. 2c). The equatorial Atlantic is warmest in March–April (Fig. 2b), corresponding to a seasonal cycle with a fast cooling during the onset phase of the ACT and slower warming after it has reached its maximum spatial extent (Caniaux et al., 2011; Brandt et al., 2011). At the eastern boundary between the Equator and 15° S, the lowest sea surface temperatures (SSTs) near the coast are found between July and September. At the northern boundary of the Gulf of Guinea, winds strengthen as well during boreal summer in accordance with northward migration of the ITCZ and the development of the West African monsoon, resulting in upwelling-favourable westerlies along the Ghanaian coast. The lowest SST near the coast is found in July–August (Fig. 2c).

In the tropical Atlantic, the thermocline depth can often be associated with the depth of the nitracline. An upward movement of the thermocline thus marks upward vertical advection of nitrate, fuelling biological productivity (Radenac et al., 2020). Besides local wind forcing, the propagation of equatorial and coastally trapped waves (CTWs) along the equatorial and coastal waveguides, respectively, contributes to the vertical movement of the thermocline and the nitracline. Such wave propagation can result in dynamic upwelling far away from the wave generation sites (Illig et al., 2018a, b; Bachèlery et al., 2020; Hormann and Brandt, 2009). The Hovmöller diagrams of SST and winds, as well as of chlorophyll concentration and sea surface height, show the seasonal development along the equatorial and coastal

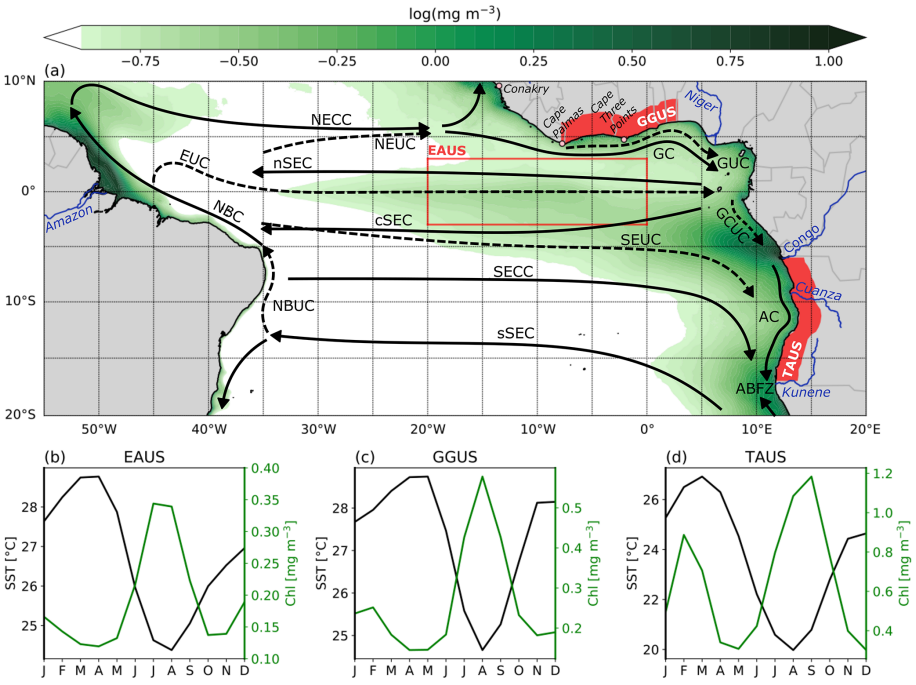

Figure 1. (a) Mean chlorophyll concentration in the tropical Atlantic with circulation schematic superimposed. Surface (solid arrows) and thermocline (dashed arrows) current branches shown are the North Equatorial Countercurrent (NECC); the North Equatorial Undercurrent (NEUC); the Guinea Undercurrent (GUC); the Guinea Current (GC); the North Brazil Undercurrent (NBUC); the North Brazil Current (NBC); the Equatorial Undercurrent (EUC); the northern, central and southern branches of the South Equatorial Current (nSEC, cSEC and sSEC); the South Equatorial Undercurrent (SEUC); the South Equatorial Countercurrent (SECC); the Gabon–Congo Undercurrent (GCUC) and the Angola Current (AC). Also marked are the Angola–Benguela Frontal Zone (ABFZ) at about 17° S and the rivers Amazon, Niger, Congo, Cuanza and Kunene. The red box marks the equatorial Atlantic upwelling system (EAUS; 3° N–3° S, 20–0° W). Red patches mark the coastal extent of the Gulf of Guinea upwelling system (GGUS; 8° W–3° E, 1° width coastal band) and the tropical Angolan upwelling system (TAUS; 6–17° S, 1° width coastal band). The mean seasonal cycle of SST and chlorophyll is shown for EAUS **(b)**, GGUS **(c)** and TAUS **(d)**. SST data are from the Microwave OI SST product, and chlorophyll data are from Copernicus-GlobColour, both averaged for 1998–2020.

waveguides in the Northern (Fig. 3) and Southern (Fig. 4) hemispheres, respectively. Primary cooling in the EAUS can be identified following the enhancement of upwelling-favouring easterly winds along almost the whole Equator in May–June (Weingartner and Weisberg, 1991). A secondary cooling occurs in November–December (Jouanno et al., 2011a; Okumura and Xie, 2006). In the GGUS, where SST reaches minimum values in August (Fig. 3a), upwelling-favouring westerly winds contribute to local cooling (Djakouré et al., 2017). Contrarily, the southerly winds in the TAUS are particularly weak during the phases of the coldest sea surface (Fig. 4a) (Körner et al., 2023; Ostrowski et al., 2009). Biological productivity (or chlorophyll concentration) is generally enhanced during periods of depressed sea surface height or correspondingly during periods of elevated thermocline (Fig. 4b).

In this review, we focus on the upper-ocean seasonal cycle in the three eastern-basin upwelling systems of the tropical Atlantic between about 10° N and 20° S, the physical forcing driving the upwelling, the upward nutrient supply, and the resulting biological productivity. Section 2 focusses on equatorial upwelling, Sect. 3 focuses on the Gulf of Guinea coastal upwelling, and Sect. 4 focuses on the tropical Angolan upwelling. In Sect. 5, we discuss longer-term changes and global warming and its relation to the seasonal cycle of upwelling, and finally, in Sect. 6, we provide a conclusion and outlook.

2 Equatorial upwelling

The equatorial upwelling transports cool, nutrient-rich waters toward the surface of the equatorial Atlantic. Its influence at the surface is more pronounced in the eastern part of the basin, where it gives rise to the development of the ACT. Its intensity is modulated by a seasonal cycle composed of an annual and a semiannual component, with a primary SST minimum in July–August and a secondary minimum in November–December (Fig. 3; Okumura and Xie, 2006; Jouanno et al., 2011a). The first insights into the seasonal evolution were obtained from observational studies in the 1980s, revealing a close link between seasonal surface cool-

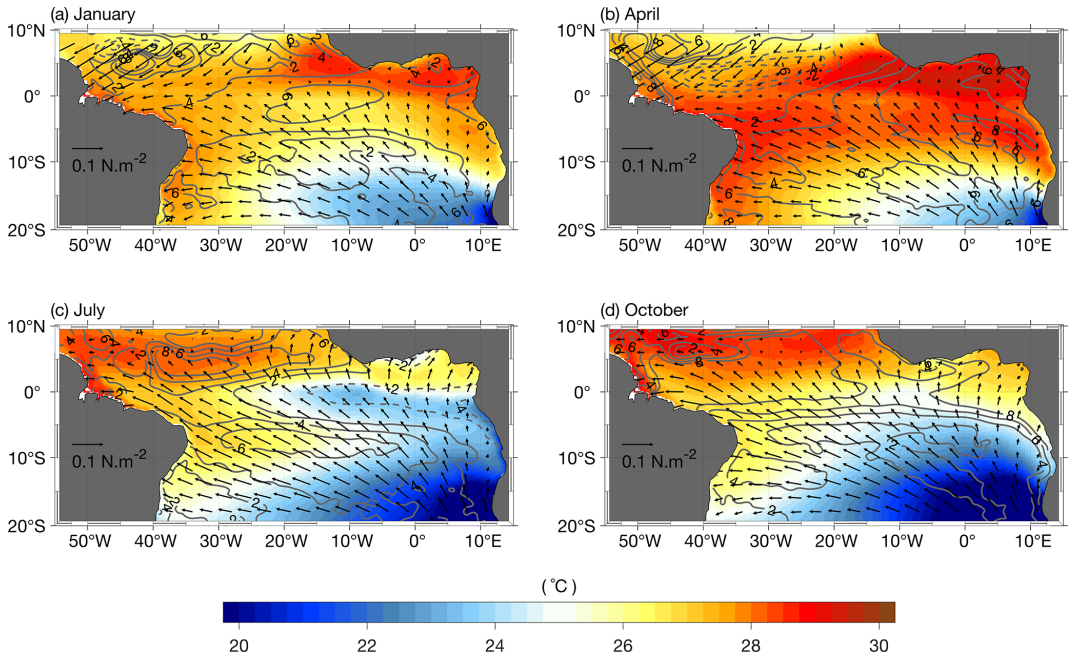

Figure 2. Monthly mean sea surface temperature (SST; colour shading), sea level anomaly (contour lines; unit is cm) and wind stress (arrows) during **(a)** January, **(b)** April, **(c)** July and **(d)** October. SST data are from OI-SST (https://www.esrl.noaa.gov/psd/data/gridded/, last access: 11 April 2023), surface wind stress data are from ERA5 (https://cds.climate.copernicus.eu/, last access: 11 April 2023), and sea level anomaly data are from the European Union Copernicus Marine Service Information (http://marine.copernicus.eu/, last access: 11 April 2023). The data are averaged between 1982–2021.

ing and vertical movements of the thermocline (Merle, 1980; Voituriez et al., 1982). Indeed, periods of surface cooling in the eastern equatorial Atlantic are in phase with the thermocline upwelling in May–June and November (Fig. 5). By using forced ocean models, Philander and Pacanowski (1981) have revealed variations of the equatorial thermocline as forced by the seasonal cycle of the wind stress; stronger easterlies result in a stronger uplift of the thermocline in the eastern equatorial Atlantic. These authors discussed the response of the Atlantic Ocean to the seasonal wind forcing as an equilibrium response that can be understood as a succession of steady states. However, such an equilibrium response requires the dominance of low-baroclinic-mode equatorial Kelvin and Rossby waves that propagate fast enough to adjust the thermocline to the wind forcing within the seasonal cycle (Ding et al., 2009; Hormann and Brandt, 2009; Philander and Pacanowski, 1986, 1981). Beside the eastern thermocline uplift, the equatorial easterlies force a strong eastward thermocline flow, the EUC, that supplies the upwelling in the eastern equatorial Atlantic (Johns et al., 2014; Schott et al., 1998).

The equatorial upwelling is an integral part of the STCs that are driven by the easterlies away from the Equator. The meridional divergence calculated from the Ekman transports at about 10° S and 10° N is about 20 Sv (Schott et al., 2004; Tuchen et al., 2019). Easterlies at the Equator additionally result in equatorial upwelling that is part of the tropical cells (Perez et al., 2014). Tropical cells are similar overturning circulations as the STCs, but these are confined to only the upper 100 m, with upwelling at the Equator and downwelling at latitudes of about ± 3–5°. The annual mean tropical cells in the central tropical Atlantic are found to be asymmetric with respect to the Equator; the northern cell extends into the Southern Hemisphere. This behaviour can be explained by the presence of southerly winds that peak during boreal autumn and that drive a cross-equatorial northward surface flow at the Equator (Heukamp et al., 2022). This circulation feature, often referred to as the equatorial roll, has maximum southward return flow at about 50 m depth and upwelling and downwelling slightly south and north of the Equator, respectively. The upwelling velocity in the equatorial Atlantic is often estimated from local wind forcing as the sum of the Ekman pumping due to the zonal wind stress, meridional wind stress, wind stress divergence and wind stress curl (Caniaux et al., 2011). By using a realistic model of the equatorial Atlantic, including in particular the full dynamic response to the wind forcing, Giordani and Caniaux (2011) show that the dominant term driving the equatorial upwelling is still the forcing by zonal wind stress. The importance of the forcing by the wind stress divergence and the wind stress curl is, however, overestimated and underestimated, respectively, in the Ekman theory compared to in the applied dynamic model.

Over the past decade, several studies have revealed that turbulent mixing is the strongest cooling term of the mixed-

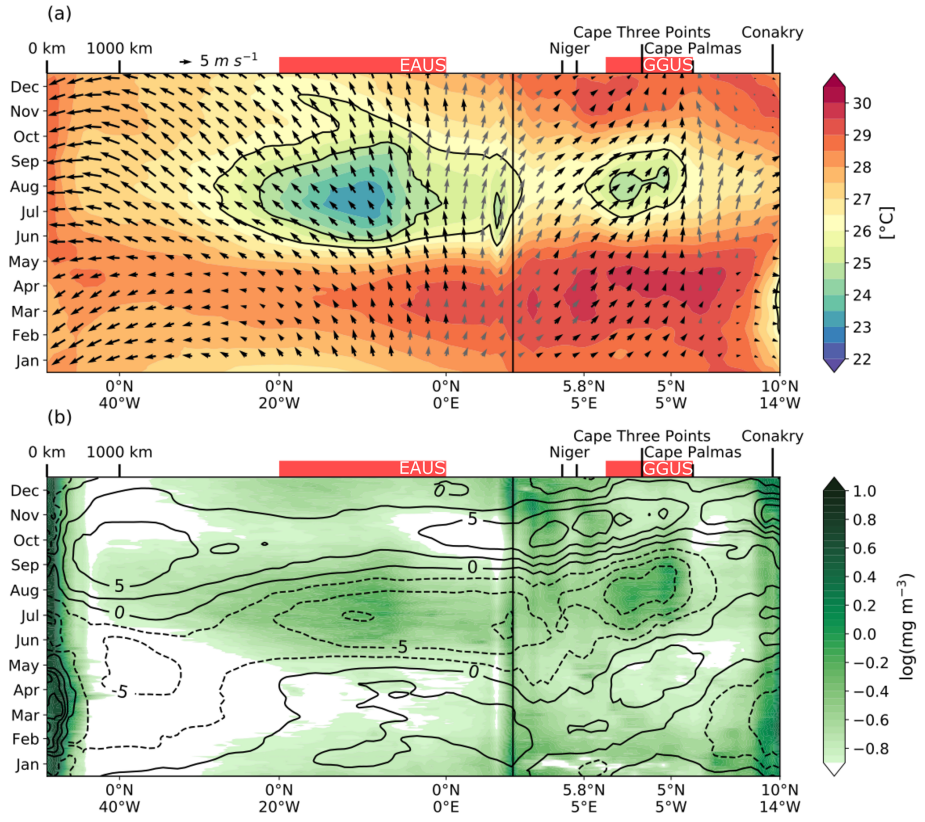

Figure 3. Seasonal cycle of **(a)** sea surface temperature (shading) and wind stress (arrows) and **(b)** chlorophyll concentration (shading) and sea level anomaly (contour lines; unit is cm) along the equatorial (left of the vertical black lines) and Gulf of Guinea coastal waveguides (right of the vertical black lines). Marks at the lower x axis give geographic coordinates, and marks at the upper x axis give a scale for the distance and geographic locations along the waveguides. Also included in **(a)** are contours of the 25 and 26 °C isotherms to highlight equatorial and coastal upwelling. Upwelling- and downwelling-favourable winds in **(a)** are marked by black and grey arrows, respectively. Upwelling-favourable winds have an eastward component along the equatorial waveguide and an alongshore, equatorward component along the coastal waveguide. Positive and negative sea level anomalies in **(b)** are marked by solid and dashed contour lines, respectively; the mean sea level anomaly is removed. SST data are from the Microwave OI SST product, wind data are from CCMP, chlorophyll data are from Copernicus-GlobColour, and sea level anomaly data are from Copernicus DUCAS. All data are averaged for 1998–2020 within a 1° band along the Equator (±0.5°) and within a 1° distance along the coast.

layer heat budget during the onset of the ACT and sets the spatial distribution and temporal variability of equatorial surface cooling (e.g. Jouanno et al., 2011a). Turbulent mixing at the base of the mixed layer that drives heat flux out of the mixed layer into the deeper ocean is dominantly induced by the vertical shear of the zonal equatorial currents, that is the westward South Equatorial Current at the surface and the eastward EUC at the thermocline level (Hummels et al., 2013). Different processes such as zonal currents seasonally varying in strength and core depth, vertical shear associated with intraseasonal waves, the seasonally varying meridional circulation, and the deep-cycle turbulence contribute to the spatial and temporal variability of equatorial mixing (Moum et al., 2022; Heukamp et al., 2022). Using the diapycnal heat flux derived from observations, the seasonal mixed-layer heat budget at the Equator could be closed to a large extent, and the seasonal development of the mixed-layer temperatures could be reasonably well explained (Hummels et al., 2014).

An important consequence of upwelling is the increase in biological productivity that is primarily dependent on nitrate supply (Herbland and Voituriez, 1979; Loukos and Memery, 1999; Radenac et al., 2020; Moore et al., 2004). There is a strong similarity between the seasonal cycles of phytoplankton concentration and SST in the cold-tongue area (Fig. 3) (Jouanno et al., 2011b), suggesting that the same physical processes control the downward heat flux out of the mixed layer and the upward supply of nitrate to the euphotic layer. This was confirmed by the analysis of repeated sections of PIRATA service cruises and outputs from a coupled physical–biogeochemical model (Radenac et al., 2020). Surface chlorophyll concentrations in the ACT peak in July–August and exhibit a secondary maximum in December–January (Figs. 3b and 4b, 5c). Radenac et al. (2020) showed

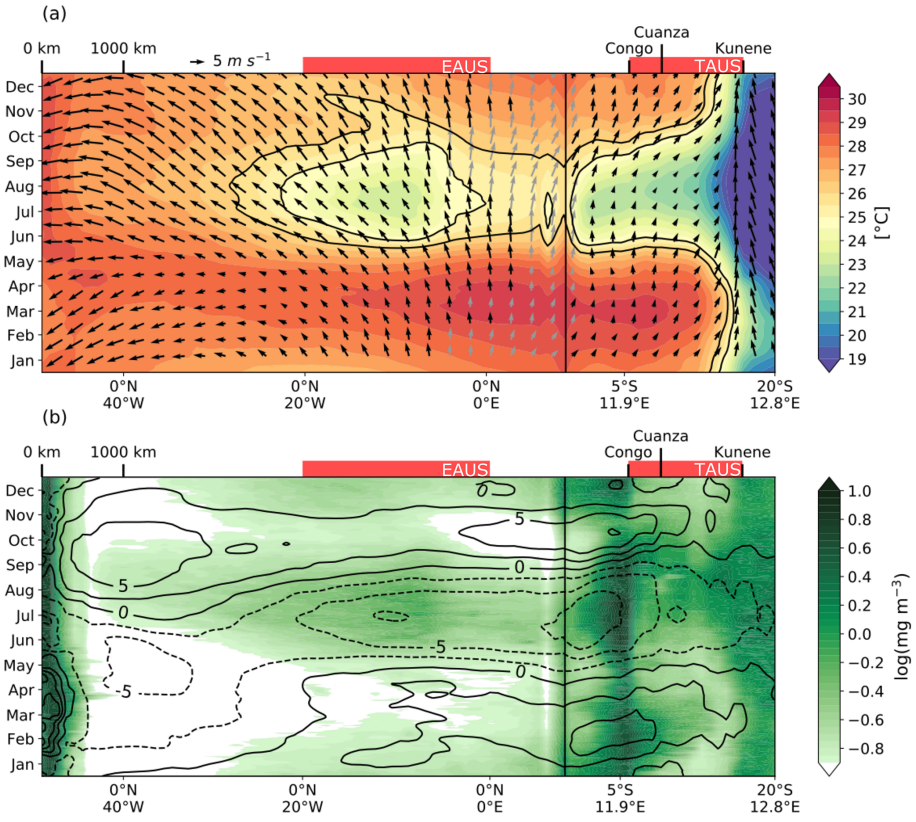

Figure 4. Same as Fig. 3 but along the southwest African coastal waveguide (right of the vertical black lines).

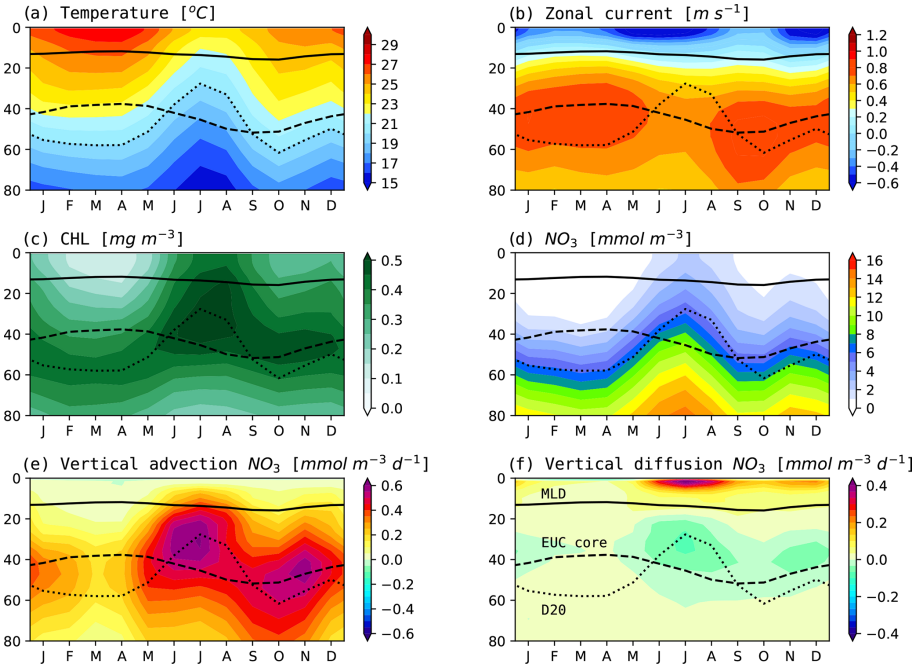

Figure 5. Seasonal cycle of vertical profiles of **(a)** temperature, **(b)** zonal velocity, **(c)** chlorophyll, **(d)** nitrate, **(e)** vertical advection and **(f)** vertical diffusion, horizontally averaged at 1.5° S–0.5° N, 20–5° W. The depths of the mixed layer (upper solid line), of the EUC core (dashed line) and of the 20 °C isotherm (dotted line) are indicated. Model output is taken from Radenac et al. (2020).

that the primary phytoplankton bloom in July–August is due to a strong vertical nitrate input to the equatorial euphotic layer in May–July, and the secondary bloom in December is due to a shorter, moderate input in November–December (Fig. 5d). Their analysis of the nitrate balance in the upper ocean suggests that vertical advection controls the vertical movement of the nitracline and that vertical diffusion allows nitrate to reach the mixed layer (Fig. 5e, f). However, as already noted by Monger et al. (1997), the phytoplankton concentration levels remain high beyond the primary bloom period in July–August despite the fact that the thermocline and nitracline drop back to the pre-uplift depth in September. Radenac et al. (2020) pointed towards a different behaviour of the EUC during boreal spring and autumn, where a shallow EUC during boreal spring might prevent upward mixing of nitrate compared to the deep phase of the EUC during boreal autumn, when nitrate more easily reaches into the shear zone above the EUC core (Fig. 5). However, in addition, the equatorial role being at maximum strength during boreal autumn (Heukamp et al., 2022) might contribute to the nitrate supply into the mixed layer by upwelling slightly south of the Equator.

Analysis of the PIRATA shipboard sections and model outputs in Radenac et al. (2020) showed that waters transported eastward by the EUC have, in general, relatively low nitrate concentrations compared to nearby water bodies to the north and south. This is most likely due to the source waters of the EUC that arrive from the oligotrophic layers of the subtropical South Atlantic (Schott et al., 1998; Johns et al., 2014; Tuchen et al., 2022a). The model simulations by Radenac et al. (2020) also revealed that the EUC core does not follow the thermocline depth (as defined as the 20 °C isotherm; Fig. 5). While in the eastern equatorial Atlantic, the vertical migration of the thermocline undergoes a semi-annual cycle in accordance with the local wind forcing, the EUC core depth has a dominant annual cycle (Brandt et al., 2014). This non-equilibrium response of the equatorial Atlantic to the seasonal wind forcing could be explained by resonant equatorial basin modes composed of eastward- and westward-propagating equatorial Kelvin and Rossby waves, respectively (Brandt et al., 2016). As the thermocline depth is a good proxy of the nitracline (Fig. 5d), the EUC transports elevated nitrate and phytoplankton concentrations when the EUC core is close to or deeper than the thermocline or nitracline, which is the case during July–August and, to a lesser extent, in December (Fig. 5).

Measurements along the Equator during two cruises in boreal autumn (Fig. 6a) and boreal spring (Fig. 6b) reveal the basin-wide character of the upward and downward movement of the EUC core relative to the thermocline depths. During boreal autumn, the EUC core closely follows the thermocline, while during boreal spring, it is located clearly above the thermocline. This behaviour can be associated with the resonance of the equatorial basin at the annual period. The period of a resonant equatorial basin mode is given by the total travel time of an equatorial Kelvin wave and its reflected equatorial Rossby wave. For the width of the equatorial Atlantic basin, the resonance period of the fourth baroclinic mode is close to the annual cycle (Brandt et al., 2016). This basin mode is associated with the maximum eastward velocity in the near-surface layer in boreal spring and the maximum westward flow in boreal autumn. A specific consequence of the relative movement of the EUC core and thermocline depths is that the thermocline and thus the nitracline during part of the year vertically migrate into the shear zone above the EUC core. As the upper shear zone of the EUC supports strongly elevated turbulent mixing (Hummels et al., 2014, 2013; Jouanno et al., 2011b; Moum et al., 2022), enhanced upward nutrient flux occurs during those periods. Such behaviour was identified in the model study of Radenac et al. (2020), showing a maximum in the near-surface diffusive nitrate flux into the mixed layer in July–August and a secondary maximum in November–December (Fig. 5f).

Beside a seasonal cycle, the productivity on the Equator shows elevated intraseasonal and shorter-term variability. In particular, tropical instability waves (TIWs) and wind-forced intraseasonal waves play an important role in stimulating local productivity due to meridional advection of both nitrate and chlorophyll, as well as the events of enhanced vertical advection and mixing (Athie and Marin, 2008; Menkes et al., 2002; Jouanno et al., 2013). TIWs are found to be associated with strong mixing events (Moum et al., 2009) or the generation of fronts (Warner et al., 2018), both of which can drive upward nutrient supply. Resulting high-productivity events could be observed during the boreal autumn cruise (Fig. 6a, c) that took place shortly after the seasonal maximum of the TIW activity (Sherman et al., 2022).

3 Gulf of Guinea upwelling

In the Gulf of Guinea, coastal upwelling occurs seasonally along the northern coast, between 10° W and 5° E, from Côte d'Ivoire to Nigeria (Hardman-Mountford and McGlade, 2003). It plays a key role in primary production and in local fisheries and is therefore of large socio-economic importance for the bordering countries (Koné et al., 2017; Amemou et al., 2020). SST variability in the GGUS is suggested to modulate the amplitude of the African monsoon and thus has an influence on regional climate (Caniaux et al., 2011; Djakouré et al., 2017). The GGUS is composed of two main upwelling cells, an eastern cell east of Cape Three Points (4°44′ N, 2°05′ W) and a western cell east of Cape Palmas (4°22′ N, 7°43′ W), that are marked by regions of reduced SST near the coast in terms of satellite data (Fig. 3a; Wiafe and Nyadjro, 2015).

Different physical processes have been proposed to explain the presence of the coastal upwelling in the GGUS. In early studies, the coastal upwelling has been related to the strengthening of the geostrophic coastal current by lo-

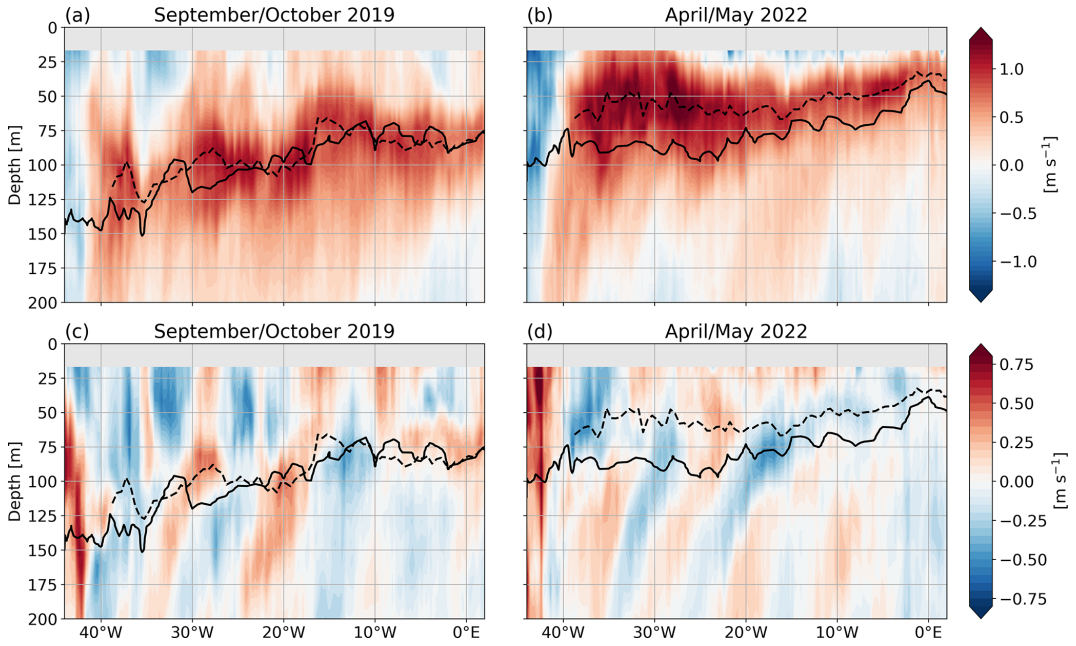

Figure 6. Zonal **(a, b)** and meridional **(c, d)** velocity measured along the Equator in September–October 2019 **(a, c)** and in April–May 2022 **(b, d)**. Note the different colour scales for the zonal and meridional velocities. EUC core depth is marked by dashed lines, and the 20 °C isotherm (as a proxy of the thermocline and the nitracline) is marked by the solid lines.

cal and remote wind forcing. Indeed, the seasonal strengthening in the eastward-flowing Guinea Current contributes to enhance the meridional tilt of the thermocline, thereby bringing cooler subsurface waters near the coast closer to the surface (Colin et al., 1993; Ingham, 1970; Bakun, 1978; Philander, 1979). The link between SST and wind stress curl in the GGUS was first suggested by Katz and Garzoli (1982) and Garzoli and Katz (1983). By using a model of the tropical Atlantic, Philander and Pacanowski (1986) showed the influence of both wind components and the wind stress curl on the upwelling in the GGUS. Additionally, Marchal and Picaut (1977) analysed isotherm displacements between Ghana and Côte d'Ivoire and suggested that vertical pumping by cyclonic eddies generated downstream of Cape Three Points and Cape Palmas could explain the upwelling of cool waters. However, modelling results by Djakouré et al. (2014) did not confirm that the cyclonic eddies generated downstream of the capes contribute to the upwelling. Instead, Djakouré et al. (2014, 2017) suggested that the upwelling downstream of Cape Palmas is associated with the nonlinear dynamics of the Guinea Current. The inclusion of the nonlinearity in the momentum equations of their model results in an inertial detachment of the Guinea Current from the coast after passing Cape Palmas. The geostrophic adjustment at the coastward flank of the current then leads to thermocline upwelling downstream of Cape Palmas. It is worth noting that the thermocline depth and the strength of the coastal current, and thus the upwelling, are all under the seasonal remote influence of the equatorial ocean through the propagation of equatorial Kelvin and Rossby waves and also of CTWs (Moore et al., 1978; Clarke, 1979; Servain et al., 1982; Picaut, 1983; Adamec and Obrien, 1978). Such remote influence is also indicated by the seasonal cycle of the sea level anomaly along the equatorial and coastal waveguides (Fig. 3b) and was found for intraseasonal wave propagations as well (Polo et al., 2008; Imbol Koungue and Brandt, 2021).

By using a model of the tropical Atlantic with an embedded high-resolution nest for the Gulf of Guinea, Djakouré et al. (2014, 2017) performed sensitivity experiments to identify the dominant processes driving the seasonal upwelling in GGUS. The sensitivity includes experiments with a changed coastline without the capes (Djakouré et al., 2014) and with the nonlinear terms in the momentum equations responsible for the advection of momentum removed (Djakouré et al., 2017). The spatial distribution of the mean SST for the major upwelling season (July–September) is shown for their reference simulation in Fig. 7. A comparison of the sensitivity experiments with the reference simulations (Fig. 8) shows that the sea surface during boreal summer is still colder than 25 °C (chosen as a threshold for the presence of coastal upwelling) when the capes are removed (Fig. 8b). The western upwelling cell disappears only when the nonlinear terms in the momentum equations are removed and when the Guinea Current is trapped at the coast (Fig. 8c).

In each of these configurations, the thermocline depth, superimposed on the SST in Fig. 8, is closest to the surface during the upwelling season. During this period, in the simulation without capes, the thermocline has a structure that is

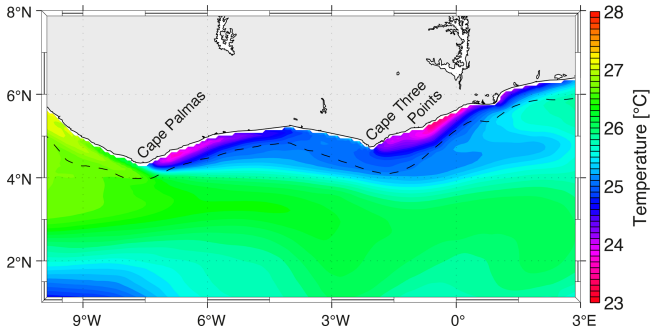

Figure 7. Mean SST (°C) for the major cold season (July–September) of the reference experiment by Djakouré et al. (2017). The dashed line represents the 1000 m isobath. Model output is taken from Djakouré et al. (2017).

almost identical to that of the realistic configuration. However, the thermocline depth is always larger than 20 m in the simulation without capes and is thus deeper than in the reference simulation. In the simulation without nonlinear terms, the deepening of the thermocline relative to the reference simulation is stronger in the western upwelling cell than in the eastern upwelling cell (west and east of Cape Three Points, respectively), resulting in strongly reduced cooling in the western upwelling cell when advection of momentum is removed. The sensitivity experiments demonstrated that advection of momentum is the main contributor to the vertical pumping of the western upwelling cell; the cooling of the eastern upwelling cell is mainly associated with the offshore Ekman transport (Djakouré et al., 2017).

In the eastern part of the GGUS that is dominantly wind-driven (Fig. 3a), coastal cooling weakens toward the east while approaching the Niger River mouth (Fig. 9). Earlier studies have shown that onshore geostrophic flow can compensate for wind-driven offshore transport, thus reducing upwelling in some regions (Marchesiello and Estrade, 2010; Rossi et al., 2013). Using a realistic regional model configuration, Ekman and geostrophic coastal upwelling indices were compared to coastal vertical velocities along the northern Gulf of Guinea coast during the boreal summer season (Alory et al., 2021). Indeed, the upwelling indices were able to explain a large part of the vertical velocity variations along the coast. They also showed that wind-forced coastal upwelling is reduced by about 50 % due to onshore geostrophic flow east of 1° E (Fig. 9a). Note that the Ekman coastal upwelling index shown in Fig. 9a only takes into account the Ekman transport, as Ekman pumping has little influence in this region (Wiafe and Nyadjro, 2015). The onshore geostrophic flow is associated with a sea level slope that increases toward the east. It is driven by density differences along the coast, from relatively cool and salty waters in the upwelling core east of Cape Three Points (Fig. 7) to warm and fresh waters in the Niger River plume, and largely compensates for offshore Ekman transport and therefore reduces upwelling (Fig. 9a).

The comparison of a reference simulation with a simulation in which river runoff is removed revealed that the Niger River discharge contributes to inducing an onshore geostrophic surface flow but additionally causes a thinning of the mixed layer. Overall, there is no net effect of the river discharge on the near-surface geostrophic transport from which the geostrophic upwelling index is derived. Nevertheless, the Niger River discharge induces a coastal warming that reaches 1 °C near 2° E (Fig. 9b), which likely is the result of reduced turbulent mixing by the enhanced salt stratification (Alory et al., 2021). The summer upwelling season corresponds to both a maximum thinning of the mixed layer and a maximum surface chlorophyll concentration along the coast (Toualy et al., 2022). Riverine nutrient inputs may be more or less compensated for by a reduced upward nutrient flux due to discharge-driven increased stratification, as there is no strong chlorophyll signal in the plume region (Fig. 1).

4 Tropical Angolan upwelling

The Angolan waters host a highly productive ecosystem, the TAUS (Fig. 1). Located in the Southern Hemisphere between the Congo River mouth at 6° S and the Angola–Benguela frontal zone at about 17° S, the TAUS is of great socio-economic importance for local communities. Fishing supplies about 25 % of the total animal protein intake of the Angolan population and is critical for economic security (Hutchings et al., 2009; Sowman and Cardoso, 2010; FAO, 2022). The productivity in the TAUS undergoes a distinct seasonal cycle (Fig. 4). In the TAUS, during austral winter, maximum productivity is observed at the same time that the lowest SST and the strongest cross-shore temperature gradient are present (Tchipalanga et al., 2018a; Awo et al., 2022; Körner et al., 2023). In contrast to other eastern-boundary upwelling systems, the seasonality of the productivity in the TAUS cannot be explained by local wind forcing (Ostrowski et al., 2009). Prevailing southerly winds in the TAUS are generally weak throughout the year (Fig. 4a). The seasonal cycles of neither alongshore wind stress nor the wind stress curl are in phase with the seasonal cycle in terms of productivity, suggesting that other mechanisms drive the productivity seasonality in the TAUS (Körner et al., 2023).

One of the key dynamics modulating the TAUS on different timescales is the passage of CTWs (Bachèlery et al., 2016a; Kopte et al., 2018, 2017; Illig et al., 2018b; Tchipalanga et al., 2018a; Awo et al., 2022; Körner et al., 2023). CTWs that propagate poleward along the eastern boundary are forced remotely by wind fluctuations along the Equator or locally by winds at the eastern boundary. Sea level satellite observations reveal the seasonal passage of four remotely forced CTWs throughout the year (Fig. 4b; Rouault, 2012; Tchipalanga et al., 2018a). A downwelling

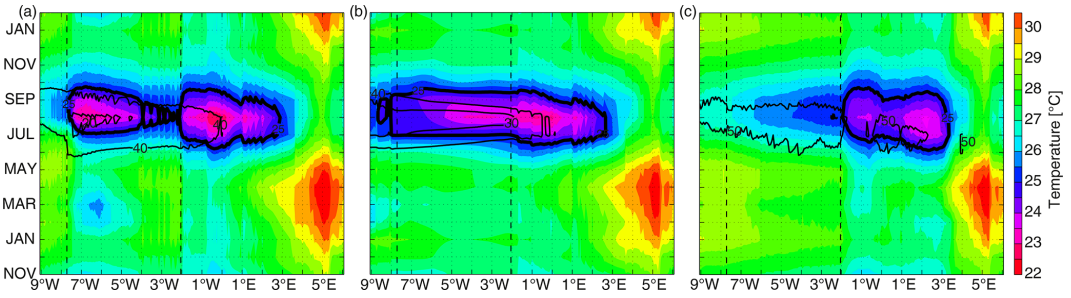

Figure 8. Hovmöller diagrams of SST (°C) along the coast of the GGUS from 9° W to 6° E of **(a)** the reference experiment and of the idealized experiments **(b)** without capes and **(c)** without inertial terms. The thermocline depth (20 °C isotherm) is superimposed (thin contour lines; unit is m). The vertical dashed black lines represent the longitude of Cape Palmas and Cape Three Points – see Fig. 7. The time axis in months extends from November to February of the following year. The 25 °C isotherm is additionally marked to highlight the coastal upwelling (thick contour lines). Model output is taken from Djakouré et al. (2014, 2017).

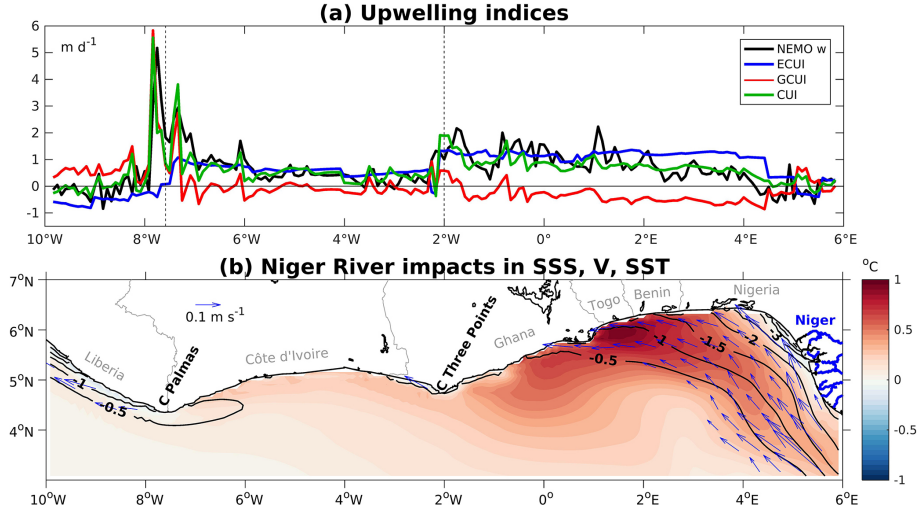

Figure 9. (a) Climatological mean (2010–2017) of boreal summer (July–September) coastal upwelling index (CUI – green line), defined as the sum of Ekman (ECUI – blue line) and geostrophic (GCUI – red lines) coastal upwelling indices, compared with coastal vertical velocity at the base of the mixed layer in the reference NEMO simulation (black line). The correlation between the CUI and vertical velocities is 0.72. Vertical dashed lines indicate the location of Cape Palmas and Cape Three Points. **(b)** River effects on boreal summer sea surface salinity (contour lines), surface geostrophic current (arrows) and sea surface temperature (colour shadings) in terms of a difference between the NEMO reference and a runoff-free simulation. Model output is taken from Alory et al. (2021).

CTW marked by anomalously high sea level arrives at the Angolan coast in March, followed by an upwelling CTW marked by anomalously low sea level in June–July. A secondary downwelling CTW propagates along the Angolan coast in October, followed by a secondary upwelling CTW in December–January. The main component of the eastern boundary circulation in the TAUS is the poleward Angola Current (Kopte et al., 2017; Siegfried et al., 2019). Its variability is linked to equatorial ocean dynamics via the propagations of CTWs at different timescales (Kopte et al., 2018, 2017; Imbol Koungue and Brandt, 2021). On seasonal timescales, the poleward velocities of the Angola Current peak in October, with a secondary maximum in February (Kopte et al., 2017).

The hydrographic conditions in the TAUS undergo distinct seasonal changes (Fig. 10). Conductivity, temperature and depth (CTD) data from 15 years of biannual research cruises of the Nansen programme (Tchipalanga et al., 2018a) illustrate the seasonal differences between the primary downwelling phase in late austral summer and the primary upwelling phase in austral winter (Fig. 10). In late austral summer (February–April), the cross-shelf section derived from data averaged between 10 and 12° S shows warm surface waters and a subsurface salinity maximum below low-salinity surface water. The subsurface salinity maximum is absent in austral winter (June–August). The isopycnals show evidence of downwelling and upwelling, as they bend downward towards the shore in late austral summer and upward in austral winter. Furthermore, the isopycnals undergo a vertical dis-

placement between the seasons (the 26.2 kg m^{-3} isopycnal moves vertically by about 50 m). The vertical displacement of the permanent thermocline can be attributed to the passage of CTWs. The seasonal passage of four CTWs induces a semiannual cycle in the vertical isopycnal movements (Kopte et al., 2017; Rouault, 2012).

To understand the changes in SST in the TAUS, one has to account for processes other than the passage of CTWs. The SST which shows an annual cycle is dominantly driven by the surface heat fluxes. The advection of warm water by the Angola Current plays only a minor role (Körner et al., 2023). In the TAUS, SST is reduced in a narrow strip along the coast compared to further offshore (Fig. 2). The resulting negative cross-shore SST gradient has a semiannual cycle and is strongest between April and September, with a secondary maximum in December–January. The cross-shore SST gradient can be explained by neither surface heat fluxes which act to dampen the spatial SST differences nor the weak horizontal heat advection. Ocean turbulence data revealed that turbulent mixing across the base of the mixed layer is strongest in shallow waters (water depths shallower than 75 m) and is capable of setting up the negative cross-shore SST gradient. The semiannual cycle of the gradient can be explained by turbulent mixing that acts upon seasonally different stratifications (Körner et al., 2023), as discussed below.

In contrast to SST, sea surface salinity (SSS) in the TAUS undergoes a semiannual cycle. Fresher water is found in the northern part of the TAUS in October–November and in February–March (Fig. 10; Kopte et al., 2017; Lübbecke et al., 2019; Awo et al., 2022). An important source of freshwater in the TAUS is the Congo River discharge at 6° S, with a maximum discharge into the ocean in early December (Martins and Stammer, 2022). The observed freshwater in the TAUS is controlled by meridional advection via the Angola Current and peaks in phase with the strengthening of the Angola Current (Awo et al., 2022). Indeed, the Angola Current displaces the freshwater from the Congo River plume toward the TAUS, leading to elevated stratification with low-salinity water at the surface above a subsurface salinity maximum. This strong stratification favours the subsurface advection of high-salinity water counteracting surface freshening via vertical salt advection and mixing at the base of the mixed layer (Awo et al., 2022).

Turbulent mixing is an important mechanism in the TAUS for the near-coastal cooling, upward salt flux and upward nutrient supply (Awo et al., 2022; Ostrowski et al., 2009; Körner et al., 2023). Ocean turbulence data from six research cruises are used to analyse the distribution of vertical eddy diffusivity at a cross-shelf section at 11° S (Fig. 11). The vertical eddy diffusivity is elevated near the bottom at the continental slope and shelf. Additionally, waters shallower than 75 m show enhanced diffusivities over nearly the whole water column. This finding suggests a dependence of mixing on bathymetry in the TAUS, with stronger mixing occurring in shallow waters, similarly to other upwelling systems (Schafstall et al., 2010; Perlin et al., 2005).

The elevated mixing rates in shallow waters of the TAUS can be explained by onshore propagating internal waves interacting with sloping topography. The main energy source of the internal wave field is assumed to be internal tides, which are generated by the interaction of the barotropic tide and the continental slope (Hall et al., 2013; Lamb, 2014). By applying a regional general circulation model forced solely by barotropic tides at the open boundaries, Zeng et al. (2021) found that, in the TAUS, a substantial part of the tidally generated internal wave energy propagates onshore and dissipates in shallow waters. The resulting enhanced near-shore mixing agrees well with observations. The seasonality of the spatially averaged generation, onshore flux and dissipation of internal tide energy is weak. This means that, throughout the year, roughly the same amount of energy is available for mixing in shallow waters. However, the resulting mixing acts on seasonally different background stratifications that vary due to the passage of CTWs, as well as due to surface heat and freshwater fluxes (Körner et al., 2023; Kopte et al., 2017). Zeng et al. (2021) showed that variations in the background stratification led to different effects of mixing on temperature; the sea surface in shallow waters near the coast cools more strongly during phases of weak stratification than during phases of strong stratification.

The productivity season in the TAUS is in phase with the propagation of CTWs (Fig. 4). The chlorophyll concentration peaks around 1 month after the passage of the primary upwelling CTW in austral winter. Similarly, a secondary chlorophyll peak is visible after the passage of the secondary upwelling CTW in December–January (Figs. 1 and 4). However, the exact process of how the passage of the CTWs leads to an increase in primary production remains an open question. While the sea surface cooling depends on the background stratification (Zeng et al., 2021; Körner et al., 2023), the upward nutrient supply additionally depends on the background distribution of nutrients. An increased vertical nitrate gradient during phases of upwelling CTW in areas of high mixing would result in higher upward nitrate fluxes. Such changes in the background nitrate conditions associated with upward and onshore advection of nitrate during the passage of upwelling CTWs might be able to ultimately explain the seasonal productivity signals in the TAUS.

5 Relation between upwelling seasonality and longer-term variability

The seasonal upwelling in the three upwelling systems discussed here peaks during approximately the same period, i.e. in July–September (Fig. 1b–d). The area and season most impacted by the upwelling show marked interannual variability, whether in terms of SST (Keenlyside and Latif, 2007) or phytoplankton concentration (Chenillat et al., 2021). Figure 12

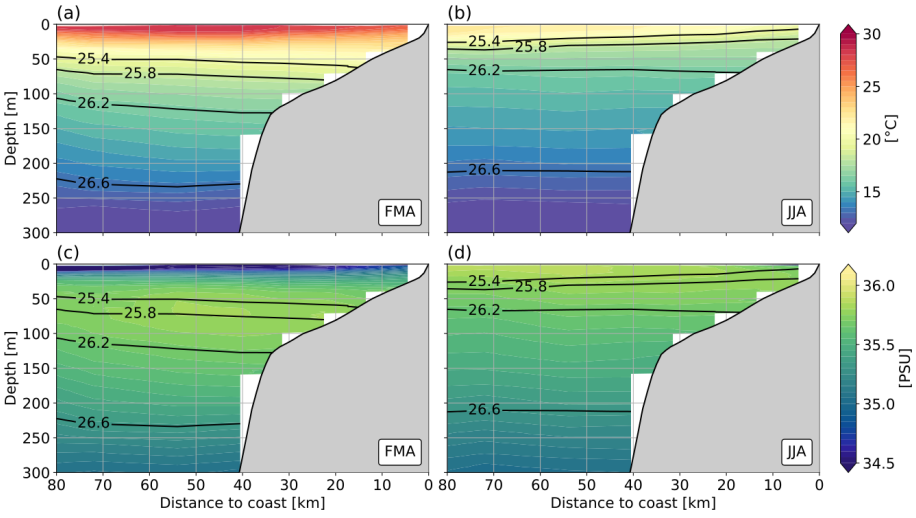

Figure 10. Hydrographic conditions between 10 and 12° S during the main downwelling phase in February–April **(a, c)** and during the main upwelling phase in June–August **(b, d)** inferred from the Nansen CTD dataset (Tchipalanga et al., 2018a). CTD data are projected on mean topography (GEBCO) between 10 and 12° S. Panels **(a)** and **(b)** show the temperature field, and panels **(c)** and **(d)** show the salinity field. Black contour lines mark potential density [kg m^{-3}]

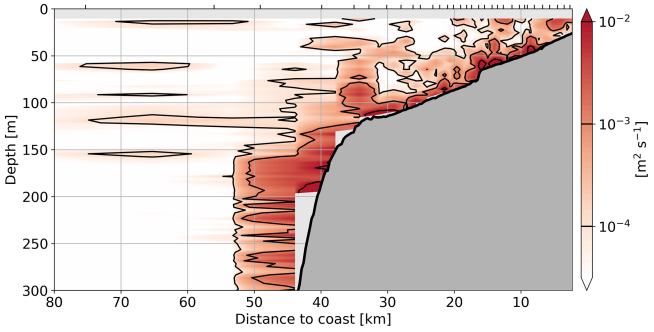

Figure 11. Vertical eddy diffusivity calculated from microstructure observation as a function of depth and distance to the coast. Measurements are taken at a section about 11° S. Eddy diffusivity is calculated for each profile individually before profiles are binned together in groups of 20 (black ticks on top mark the border of the 20-profile groups).

shows the year-to-year variability of SST of the three tropical Atlantic upwelling systems averaged for the 3 months of July–September. There are some similarities but also differences in the variability of the three upwelling systems. Outstanding is the most recent warm event in 2021 that peaked in all three upwelling systems.

The dominant climate mode in the tropical Atlantic is the Atlantic Niño (Hisard, 1980; Ruiz-Barradas et al., 2000; Lübbecke et al., 2018). It is most pronounced in the equatorial cold tongue east of 23° W and peaks during June–July (Keenlyside and Latif, 2007). Anomalous warm or cold events are thus associated with anomalous deep or shallow thermocline and correspondingly with reduced or enhanced upwelling, respectively. Atlantic Niños and Niñas are associated with SSS variability as well (Awo et al., 2018), suggesting additional forcing of the equatorial and eastern-boundary upwelling in the eastern tropical Atlantic, as the coupling between subsurface and surface is reduced for enhanced near-surface stratification. During an Atlantic Niño, the southward shift of the ITCZ brings maximum rainfall in the eastern tropical Atlantic and potentially increases the flow of surrounding rivers, affecting near-surface stratification (Awo et al., 2018; Nyadjro et al., 2022). Besides the interannual variability, decadal variability can impact the equatorial upwelling. Such variability might be associated with the changing strength of the STCs forced by off-equatorial easterlies (Rabe et al., 2008; Tuchen et al., 2020). Similarly, Brandt et al. (2021) found an intensification of the EUC for the period 2008–2018 that was linked to enhanced trade winds in the tropical North Atlantic, likely associated with the Atlantic multidecadal variability (Knight et al., 2006). Other mechanisms that are suggested to impact the strength of equatorial cooling on decadal timescales include the decadal variability of TIWs. A decadal strengthening of TIWs was found to be associated with enhanced warming of the equatorial cold tongue by lateral eddy fluxes (Tuchen et al., 2022b). Coupled climate simulations also suggest the importance of surface heat fluxes in driving interannual to decadal cold-tongue SST variability (Nnamchi et al., 2015). As discussed by Jouanno et al. (2017), such heat flux forcing is likely overemphasized due to large upper-ocean temperature biases commonly found in climate models. Chang et al. (2008) analysed the impact of a changing Atlantic meridional overturning circulation (AMOC) on the tropical Atlantic on decadal to multidecadal timescales using simulations with a climate model. These simulations showed that a weakened AMOC results in

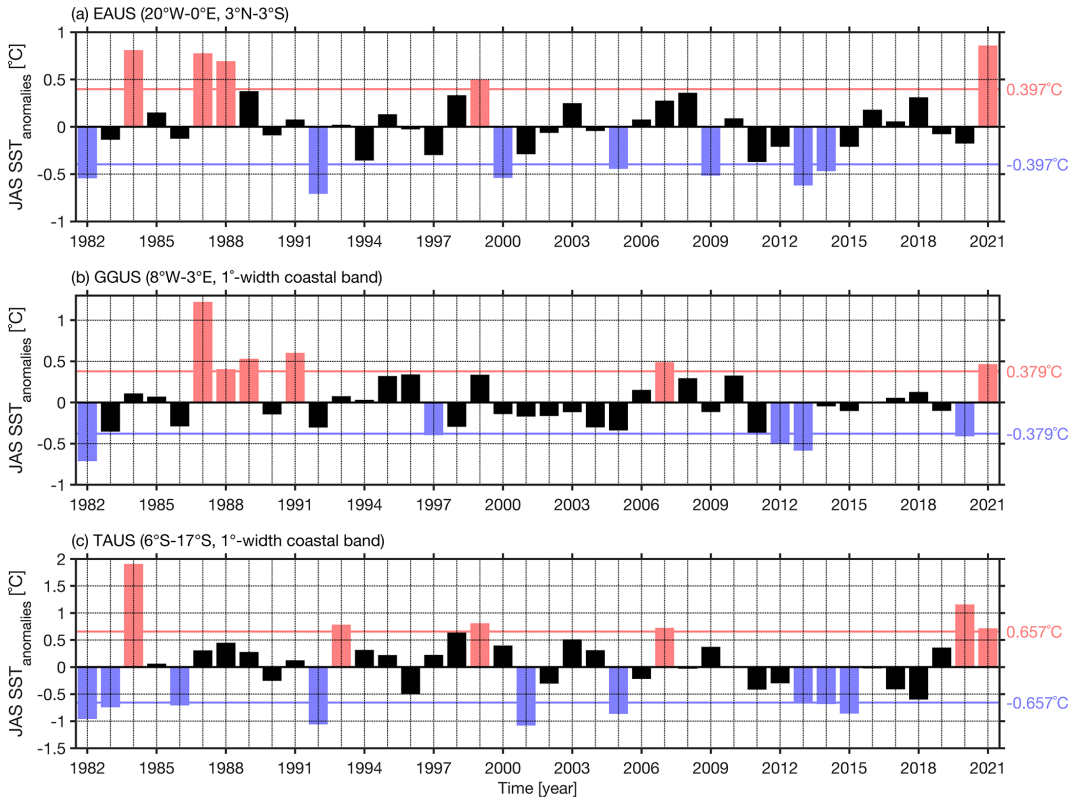

Figure 12. SST anomalies from 1982–2021 during the main upwelling season (July–September) averaged in the EAUS **(a)**, GGUS **(b)** and TAUS **(c)**. The red and blue rectangles highlight the extreme warm and cold events in the different regions, respectively. The horizontal red and blue lines show the standard deviation of the interannual SST anomalies during the main upwelling season (July–September). Anomalies are derived with respect to the seasonal cycle between 1982 and 2021 after subtracting the trend. SST data are from OI-SST (https://www.esrl.noaa.gov/psd/data/gridded/, last access: 11 April 2023).

a warmer equatorial Atlantic with a reduced seasonal cycle and interannual variability. Similarly, a weakening of interannual variability is projected under a global-warming scenario (Crespo et al., 2022; Yang et al., 2022). However, the impact of global warming or reduced AMOC on seasonal or interannual variability of productivity is highly uncertain, as even the impact on upper-ocean stratification is not coherent between different models and datasets, which is partly due to the fact that decadal trends in stratification or productivity are just emerging from the available observations (Roch et al., 2021; Sallee et al., 2021; Hammond et al., 2020).

In the GGUS, interannual variability is generally stronger in regions of strong seasonal variability, as has been documented from satellite and in situ data (Wiafe and Nyadjro, 2015; Sohou et al., 2020). Potential drivers of interannual variability are similar to drivers of seasonal changes. They include changes in the wind forcing and turbulent mixing and also remote forcing associated with the Atlantic Niño (Jouanno et al., 2017; Wade et al., 2011). Processes involved in the 2012 cold anomalies in the GGUS, one of the coldest events observed over the last 30 years (Fig. 12b), have been investigated through a model heat budget (Da-Allada et al., 2021). Results revealed that the surface cooling at Cape Palmas was driven by changes in zonal advection and increased turbulent mixing due to a strengthening of the Guinea Current and associated vertical shear, while east at Cape Three Point, where seasonal upwelling is dominated by the wind forcing, it was driven by a strengthening of the zonal wind stress that increased the offshore Ekman transport.

In the TAUS, Benguela Niños and Niñas are the dominant modes of interannual climate variability (Shannon et al., 1986). Contrary to the variability in the EAUS and GGUS, interannual variability does not reach its seasonal maximum during the main upwelling season but rather during the main downwelling season from March to May (Lübbecke et al., 2019). Still, some events are observed during austral winter, such as the 1984 Benguela Niño (Imbol Koungue et al., 2019; Shannon et al., 1986). During a Benguela Niño or Niña, SST in the TAUS can be up to 2 °C higher or lower than the climatology, respectively (Rouault et al., 2007, 2018; Imbol Koungue et al., 2019, 2021). These extreme events can have drastic consequences for the marine ecosystem (Gammelsrød et al., 1998) through modulations in coastal upwelling intensity, nutrients and oxygen content along the continen-

tal shelf (Bachèlery et al., 2016b). It can be assumed that the forcing mechanisms of Benguela Niños and Niñas are similar to those of the seasonal upwelling variability. On the one hand, winds at the Equator can generate equatorial Kelvin waves (Illig et al., 2004) that continue southward along the southwest African coast as CTWs and produce thermocline displacements along the eastern boundary (Polo et al., 2008; Imbol Koungue et al., 2017; Bachèlery et al., 2016a, 2020). On the other hand, fluctuations of local alongshore winds (Richter et al., 2010) and other local processes such as freshwater inputs (Lübbecke et al., 2019) further generate SST anomalies in the TAUS. For the satellite era, Prigent et al. (2020a) showed a weakening of interannual SST variability in the southeastern tropical Atlantic between 2000–2017 relative to 1982–1999. However, since 2018, two consecutive extreme coastal warm events have been recorded in the TAUS in 2019–2020 (Imbol Koungue et al., 2021) and in 2021 (Fig. 12c). The recent decades demonstrate a strong warming trend in the tropical Atlantic SST, with the largest warming observed in the coastal upwelling regions off southwestern Africa, including the TAUS (Tokinaga and Xie, 2011). Moreover, using observational data, Roch et al. (2021) discovered a change in upper-ocean stratification from subtropical to tropical conditions associated with a warming and freshening of the mixed layer between 2006 and 2020 in the southeastern tropical Atlantic (10–20° S, 5° W–15° E). Such changes in stratification are assumed to particularly impact the mixing-driving nitrate supply in the TAUS.

6 Conclusion and outlook

Here, we have reviewed the physical processes in three major upwelling systems of the tropical Atlantic (10° N–20° S), the EAUS, the GGUS and the TAUS, that drive the upwelling seasonality. Among them are the processes that locally impact the thermocline depth – often used as a proxy of the nitracline – such as zonal wind along the Equator, alongshore wind in coastal upwelling regions, wind stress curl or the detachment of the boundary current. Remote processes associated with the propagation of equatorial Kelvin and CTWs affect the thermocline depth in the different upwelling regions on intraseasonal, seasonal and interannual timescales as well. The processes affecting the thermocline depth can be summarized under locally and remotely driven vertical advection which is able to transfer colder and nutrient-rich waters upward to the surface during active upwelling. Additionally, diffusive fluxes associated with turbulent mixing at the base of the mixed layer and within the thermocline transport heat downward and nutrients upward. While the dominant processes driving equatorial and coastal upwelling might be identified, we are only beginning to quantify their relative importance or to understand their interactions. Examples are the nonlinear interaction of locally and remotely forced boundary current variability and horizontal density anomalies or topography (Mosquera-Vasquez et al., 2014; Kämpf, 2007), the importance and characteristics of different CTW modes and their specific role in the vertical advection of nutrients (Bachèlery et al., 2020; Illig et al., 2018a, b), or the role of intraseasonal variability and the eddy field in shaping the upwelling (Tuchen et al., 2022b; Thomsen et al., 2016). With the development of extremely high-resolution ocean models, the importance of the mesoscale and of the submesoscale and also their role in mixed-layer dynamics and thermocline mixing emerged. Dedicated observational studies, particularly in eastern boundary upwelling systems, are required, focusing on these smaller-scale dynamics and aiming at understanding their impact on seasonal and longer-term changes of upwelling.

The EAUS can be characterized as a wind-driven upwelling system forced by different wind components at the Equator and off the Equator. Off-equatorial winds drive the STCs, which act on longer timescales, mostly larger than 5 years (Schott et al., 2004; Tuchen et al., 2020). How their changes affect stratification and nutrient distribution is still an open question (Duteil et al., 2014). Wind changes along the Equator generate upwelling and downwelling equatorial waves that propagate along the Equator and adjust the equatorial thermocline to reach an equilibrium with the wind forcing. Additional wave forcing originates from westward-propagating Rossby waves and their reflection at the western boundary (Foltz and McPhaden, 2010a, b) or from CTWs generated at the western boundary (Hughes et al., 2019). A very specific response of an equatorial basin is the development of a basin resonance. Due to its width and the travel time of equatorial waves, the Atlantic basin is resonant at the second and fourth baroclinic modes for the semi-annual and annual cycles, respectively. The resonance results in an EUC that vertically migrates largely independently of the thermocline (Brandt et al., 2016). During periods when the thermocline depth is shallower than the EUC core, turbulent mixing in the shear zone above the core of the EUC is essential for the downward heat flux and upward nitrate flux out of and into the mixed layer, respectively (Jouanno et al., 2011b; Hummels et al., 2014). Similar resonances are found for the Indian Ocean (Han et al., 2011), while the Pacific Ocean, due to its larger width, develops resonances at lower baroclinic modes and/or larger periods.

In the GGUS, different processes define the two upwelling centres east of Cape Palmas and east of Cape Three Points. East of Cape Palmas, the inertial detachment of the Guinea Current from the coast plays the most important role, while east of Cape Three Points, upwelling is mainly associated with the wind-forced coastal divergence (Djakouré et al., 2017). The upwelling in the TAUS, which is characterized by weak winds, is dominantly driven by a combination of remotely forced CTWs and turbulent mixing locally enhanced in shallow waters near the coast (Körner et al., 2023; Tchipalanga et al., 2018a; Rouault, 2012).

Climate warming and change might impact the upwelling in the different regions and their seasonality (amplitude and phase) differently. Most obvious are probably future changes in the wind field, e.g. a strengthening of the winds in a warming world or poleward shifts of the main wind systems (Yang et al., 2020). Changes in the stratification and mixed-layer depths are highly uncertain, with recent studies suggesting an increase of the stratification at the base of the mixed layer together with a mixed-layer deepening that is likely due to enhanced wind-driven upper-ocean turbulent mixing (Sallee et al., 2021; Roch et al., 2021). However, other processes such as lateral mixing, responsible for reducing nitrate concentrations in upwelling regions, or surface heat fluxes might contribute as well. Recently, the multidecadal increase in the strength of TIWs and associated equatorward eddy heat flux was suggested to warm the EAUS (Tuchen et al., 2022b). Such eddy fluxes generally oppose the Ekman transport in upwelling systems. Air–sea heat and buoyancy fluxes were identified as modulating such compensation in idealized model simulations (Thomsen et al., 2021), suggesting that, in a warming climate, changes in heat and freshwater fluxes also have the potential to impact the upwelling strength via its impact on lateral eddy fluxes.

The identification of climate changes in upwelling systems is a major goal that requires the maintenance and further development of the tropical Atlantic observing system (Foltz et al., 2019). In particular, coastal upwelling regions show a sparse data coverage, and the strengthening of the near-coastal observing system is a high priority. This requires close cooperation with the coastal communities to jointly develop the research agenda according to collective interests and needs. The main questions regard the often-competing role of changes in wind forcing and stratification and the role of changing eddy fluxes and buoyancy forcing. What will be the consequences of changing the upwelling amplitude and/or timing for biogeochemistry and biology? Overall, future upwelling studies require close cooperation between different research disciplines focusing on the interaction between the physical, biogeochemical and biological systems and allowing an improved assessment of ecosystem management and fisheries.

Appendix A: List of abbreviations

AMOC	Atlantic meridional overturning circulation
ACT	Atlantic cold tongue
CTD	Conductivity, temperature and depth
CTW	Coastally trapped wave
EAUS	Equatorial Atlantic upwelling system
EUC	Equatorial Undercurrent
FAO	Food and Agriculture Organization
GGUS	Gulf of Guinea upwelling system
ITCZ	Intertropical convergence zone
TAUS	Tropical Angolan upwelling system
TIWs	Tropical instability waves
SSS	Sea surface salinity
SST	Sea surface temperature
STC	Subtropical cells

Data availability. Publicly available datasets were used for this study. Chlorophyll data (1998–2020) are from the Copernicus-GlobColour dataset (https://doi.org/10.48670/moi-00281, Copernicus, 2023a). The sea level anomaly data (1998–2020) were accessed via the Copernicus Server (https://doi.org/10.48670/moi-00148, Copernicus, 2023b). Microwave OI SST and CCMP wind data (both 1998–2020) are available under https://www.remss.com (Microwave OI SST and CCMP wind data, 2023). Surface wind stress data from ERA5 were also used (https://cds.climate.copernicus.eu/, ERA5 surface wind stress data, 2023). Sections along the Equator have been produced using ADCP data from Meteor cruise M158 (https://doi.org/10.1594/PANGAEA.952101, Brandt et al., 2023a) and M181 (https://doi.org/10.1594/PANGAEA.956143, Brandt et al., 2023b) and CTD data from M158 (https://doi.org/10.1594/PANGAEA.952354, Brandt et al., 2023c) and M181 (https://doi.org/10.1594/PANGAEA.952520, Brandt et al., 2023d). Hydrographic sections in Angolan waters have been produced using the Nansen CTD dataset (https://doi.org/10.1594/PANGAEA.887163, Tchipalanga et al., 2018b).

Author contributions. PB outlined and wrote the paper. MK, RAIK, JJ, SD and GA produced the figures. All the co-authors contributed to and reviewed the paper.

Competing interests. The contact author has declared that none of the authors has any competing interests.

Disclaimer. Publisher's note: Copernicus Publications remains neutral with regard to jurisdictional claims in published maps and institutional affiliations.

Acknowledgements. We thank the captains, crews, scientists and technicians involved in the several research cruises in the tropical Atlantic that contributed to collecting data used in this study. We are grateful to Erik van Sebille and an anonymous reviewer for their helpful comments and suggestions, which helped improve the quality of this paper.

Financial support. The study was funded by EU H2020 under grant agreement no. 817578 (TRIATLAS project). It was further supported by the German Federal Ministry of Education and Research as part of the BANINO (grant no. 03F0795A) project, by the German Research Foundation through grant no. 511812462 (IM 218/1-1) and by the French Research Institute for Development (IRD) as part of the JEAI IVOARE-UP project.

The article processing charges for this open-access publication were covered by the GEOMAR Helmholtz Centre for Ocean Research Kiel.

Review statement. This paper was edited by Erik van Sebille and reviewed by Erik van Sebille and one anonymous referee.

References

Adamec, D. and Obrien, J. J.: Seasonal upwelling in Gulf of Guinea due to remote forcing, J. Phys. Oceanogr., 8, 1050–1060, https://doi.org/10.1175/1520-0485(1978)008<1050:Tsuitg>2.0.Co;2, 1978.

Alory, G., Da-Allada, C. Y., Djakouré, S., Dadou, I., Jouanno, J., and Loemba, D. P.: Coastal Upwelling Limitation by Onshore Geostrophic Flow in the Gulf of Guinea Around the Niger River Plume, Front. Mar. Sci., 7, 607216, https://doi.org/10.3389/fmars.2020.607216, 2021.

Amemou, H., Koné, V., Aman, A., and Lett, C.: Assessment of a Lagrangian model using trajectories of oceanographic drifters and fishing devices in the Tropical Atlantic Ocean, Prog. Oceanogr., 188, 102426, https://doi.org/10.1016/j.pocean.2020.102426, 2020.

Athie, G. and Marin, F.: Cross-equatorial structure and temporal modulation of intraseasonal variability at the surface of the Tropical Atlantic Ocean, J. Geophys. Res.-Oceans, 113, C08020, https://doi.org/10.1029/2007jc004332, 2008.

Awo, F. M., Alory, G., Da-Allada, C. Y., Delcroix, T., Jouanno, J., Kestenare, E., and Baloitcha, E.: Sea Surface Salinity Signature of the Tropical Atlantic Interannual Climatic Modes, J. Geophys. Res.-Oceans, 123, 7420–7437, https://doi.org/10.1029/2018jc013837, 2018.

Awo, F. M., Rouault, M., Ostrowski, M., Tomety, F. S., Da-Allada, C. Y., and Jouanno, J.: Seasonal cycle of sea surface salinity in the Angola Upwelling System, J. Geophys. Res.-Oceans, 127, e2022JC018518, https://doi.org/10.1029/2022JC018518, 2022.

Bachèlery, M. L., Illig, S., and Dadou, I.: Interannual variability in the South-East Atlantic Ocean, focusing on the Benguela Upwelling System: Remote versus local forcing, J. Geophys. Res.-Oceans, 121, 284–310, https://doi.org/10.1002/2015jc011168, 2016a.

Bachèlery, M. L., Illig, S., and Dadou, I.: Forcings of nutrient, oxygen, and primary production interannual variability in the southeast Atlantic Ocean, Geophys. Res. Lett., 43, 8617–8625, https://doi.org/10.1002/2016gl070288, 2016b.

Bachèlery, M. L., Illig, S., and Rouault, M.: Interannual coastal trapped waves in the Angola-Benguela upwelling system and Benguela Niño and Niña events, J. Marine Syst., 203, 103262, https://doi.org/10.1016/j.jmarsys.2019.103262, 2020.

Bakun, A.: Guinea Current Upwelling, Nature, 271, 147–150, https://doi.org/10.1038/271147a0, 1978.

Bakun, A.: Global Climate Change and Intensification of Coastal Ocean Upwelling, Science, 247, 198–201, https://doi.org/10.1126/science.247.4939.198, 1990.

Bourlès, B., D'Orgeville, M., Eldin, G., Gouriou, Y., Chuchla, R., DuPenhoat, Y., and Arnault, S.: On the evolution of the thermocline and subthermocline eastward currents in the Equatorial Atlantic, Geophys. Res. Lett., 29, 32.31–32.34, https://doi.org/10.1029/2002gl015098, 2002.

Brandt, P., Caniaux, G., Bourlès, B., Lazar, A., Dengler, M., Funk, A., Hormann, V., Giordani, H., and Marin, F.: Equatorial upper-ocean dynamics and their interaction with the West African monsoon, Atmos. Sci. Lett., 12, 24–30, https://doi.org/10.1002/Asl.287, 2011.

Brandt, P., Funk, A., Tantet, A., Johns, W., and Fischer, J.: The Equatorial Undercurrent in the central Atlantic and its relation to tropical Atlantic variability, Clim. Dynam., 43, 2985–2997, https://doi.org/10.1007/s00382-014-2061-4, 2014.

Brandt, P., Bange, H. W., Banyte, D., Dengler, M., Didwischus, S.-H., Fischer, T., Greatbatch, R. J., Hahn, J., Kanzow, T., Karstensen, J., Körtzinger, A., Krahmann, G., Schmidtko, S., Stramma, L., Tanhua, T., and Visbeck, M.: On the role of circulation and mixing in the ventilation of oxygen minimum zones with a focus on the eastern tropical North Atlantic, Biogeosciences, 12, 489–512, https://doi.org/10.5194/bg-12-489-2015, 2015.

Brandt, P., Claus, M., Greatbatch, R. J., Kopte, R., Toole, J. M., Johns, W. E., and Böning, C. W.: Annual and semiannual cycle of equatorial Atlantic circulation associated with basin-mode resonance, J. Phys. Oceanogr., 46, 3011–3029, https://doi.org/10.1175/Jpo-D-15-0248.1, 2016.

Brandt, P., Hahn, J., Schmidtko, S., Tuchen, F. P., Kopte, R., Kiko, R., Bourlés, B., Czeschel, R., and Dengler, M.: Atlantic Equatorial Undercurrent intensification counteracts warming-induced deoxygenation, Nat. Geosci., 14, 278–282, https://doi.org/10.1038/s41561-021-00716-1, 2021.

Brandt, P., Czeschel, R., and Krahmann, G.: ADCP current measurements (38 and 75 kHz) during METEOR cruise M158, PANGAEA [data set], https://doi.org/10.1594/PANGAEA.952101, 2023a.

Brandt, P., Czeschel, R., and Krahmann, G.: ADCP current measurements during METEOR cruise M181, PANGAEA [data set], https://doi.org/10.1594/PANGAEA.956143, 2023b.

Brandt, P., Subramaniam, A., Schmidtko, S., and Krahmann, G.: Physical oceanography (CTD) during METEOR cruise M158, PANGAEA [data set], https://doi.org/10.1594/PANGAEA.952354, 2023c.

Brandt, P., Subramaniam, A., and Krahmann, G.: Physical oceanography (CTD) during METEOR cruise M181, PANGAEA [data set], https://doi.org/10.1594/PANGAEA.952520, 2023d.

Burls, N. J., Reason, C. J. C., Penven, P., and Philander, S. G.: Similarities between the tropical Atlantic seasonal cycle and ENSO: An energetics perspective, J. Geophys. Res.-Oceans, 116, C11010, https://doi.org/10.1029/2011jc007164, 2011.

Cai, W. J., Wang, G. J., Dewitte, B., Wu, L. X., Santoso, A., Takahashi, K., Yang, Y., Carreric, A., and McPhaden, M. J.: Increased variability of eastern Pacific El Niño under greenhouse warming, Nature, 564, 201–206, https://doi.org/10.1038/s41586-018-0776-9, 2018.

Caniaux, G., Giordani, H., Redelsperger, J. L., Guichard, F., Key, E., and Wade, M.: Coupling between the Atlantic cold tongue and the West African monsoon in boreal spring and summer, J. Geophys. Res.-Oceans, 116, C04003, https://doi.org/10.1029/2010jc006570, 2011.

Chai, F., Lindley, S. T., and Barber, R. T.: Origin and maintenance of a high nitrate condition in the equatorial Pacific, Deep-

Sea Res. Pt. II, 43, 1031–1064, https://doi.org/10.1016/0967-0645(96)00029-X, 1996.

Chang, P., Zhang, R., Hazeleger, W., Wen, C., Wan, X. Q., Ji, L., Haarsma, R. J., Breugem, W. P., and Seidel, H.: Oceanic link between abrupt changes in the North Atlantic Ocean and the African monsoon, Nat. Geosci., 1, 444–448, https://doi.org/10.1038/Ngeo218, 2008.

Chenillat, F., Illig, S., Jouanno, J., Awo, F. M., Alory, G., and Brehmer, P.: How do climate modes shape the Chlorophyll-*a* interannual variability in the tropical Atlantic?, Geophys. Res. Lett., 48, e2021GL093769, https://doi.org/10.1029/2021GL093769, 2021.

Clarke, A. J.: On the generation of the seasonal coastal upwelling in the Gulf of Guinea, J. Geophys. Res.-Oceans, 84, 3743–3751, https://doi.org/10.1029/JC084iC07p03743, 1979.

Colin, C., Gallardo, Y., Chuchla, R., and Cissoko, S.: Environnements climatique et océanographique sur le plateau continental de Côte d'Ivoire, in: Environnement et ressources aquatiques de Côte d'Ivoire: 1. Le milieu marin, edited by: Le Loeuff, P., Marchal, E., and Amon Kothias, J. B., ORSTOM, Paris, 75–110, https://horizon.documentation.ird.fr/exl-doc/pleins_textes/pleins_textes_7/divers2/37710.pdf (last access: 11 April 2023), 1993.

Copernicus: Global Ocean Colour (Copernicus-GlobColour), Bio-Geo-Chemical, L4 (monthly and interpolated) from satellite observations (1997-ongoing), Copernicus [data set], https://doi.org/10.48670/moi-00281, 2023a.

Copernicus: Global Ocean Gridded L4 Sea Surface Heights and derived variables reprocessed 1993 ongoing, Copernicus [data set], https://doi.org/10.48670/moi-00148, 2023b.

Crespo, L. R., Prigent, A., Keenlyside, N., Koseki, S., Svendsen, L., Richter, I., and Sanchez-Gomez, E.: Weakening of the Atlantic Niño variability under global warming, Nat. Clim. Change, 12, 822–827, https://doi.org/10.1038/s41558-022-01453-y, 2022.

Da-Allada, C. Y., Agada, J., Baloitcha, E., Hounkonnou, M. N., Jouanno, J., and Alory, G.: Causes of the Northern Gulf of Guinea Cold Event in 2012, J. Geophys. Res.-Oceans, 126, e2021JC017627, https://doi.org/10.1029/2021JC017627, 2021.

Ding, H., Keenlyside, N. S., and Latif, M.: Seasonal cycle in the upper equatorial Atlantic Ocean, J. Geophys. Res.-Oceans, 114, C09016, https://doi.org/10.1029/2009jc005418, 2009.

Djakouré, S., Penven, P., Bourlès, B., Veitch, J., and Kone, V.: Coastally trapped eddies in the north of the Gulf of Guinea, J. Geophys. Res.-Oceans, 119, 6805–6819, https://doi.org/10.1002/2014jc010243, 2014.

Djakouré, S., Penven, P., Bourlès, B., Kone, V., and Veitch, J.: Respective roles of the Guinea Current and local winds on the coastal upwelling in the northern Gulf of Guinea, J. Phys. Oceanogr., 47, 1367–1387, https://doi.org/10.1175/Jpo-D-16-0126.1, 2017.

Duteil, O., Böning, C. W., and Oschlies, A.: Variability in subtropical-tropical cells drives oxygen levels in the tropical Pacific Ocean, Geophys. Res. Lett., 41, 8926–8934, https://doi.org/10.1002/2014gl061774, 2014.

ERA5 surface wind stress data: Climate Data Store, https://cds.climate.copernicus.eu/, last access: 11 April 2023.

FAO: Fishery and Aquaculture Country Profiles, Angola, 2020, Country Profile Fact Sheets, Fisheries and Aquaculture Division [online], Rome, https://www.fao.org/fishery/en/facp/ago?lang=en (last access: 11 April 2023), updated 7 February 2022.

Foltz, G. R. and McPhaden, M. J.: Abrupt equatorial wave-induced cooling of the Atlantic cold tongue in 2009, Geophys. Res. Lett., 37, L24605, https://doi.org/10.1029/2010gl045522, 2010a.

Foltz, G. R. and McPhaden, M. J.: Interaction between the Atlantic meridional and Nino modes, Geophys. Res. Lett., 37, L18604, https://doi.org/10.1029/2010gl044001, 2010b.

Foltz, G. R., Brandt, P., Richter, I., Rodriguez-Fonsecao, B., Hernandez, F., Dengler, M., Rodrigues, R. R., Schmidt, J. O., Yu, L., Lefevre, N., Da Cunha, L. C., McPhaden, M. J., Araujo, M., Karstensen, J., Hahn, J., Martin-Rey, M., Patricola, C. M., Poli, P., Zuidema, P., Hummels, R., Perez, R. C., Hatje, V., Lübbecke, J. F., Palo, I., Lumpkin, R., Bourlès, B., Asuquo, F. E., Lehodey, P., Conchon, A., Chang, P., Dandin, P., Schmid, C., Sutton, A., Giordani, H., Xue, Y., Illig, S., Losada, T., Grodsky, S. A., Gasparinss, F., Lees, T., Mohino, E., Nobre, P., Wanninkhof, R., Keenlyside, N., Garcon, V., Sanchez-Gomez, E., Nnamchi, H. C., Drevillon, M., Storto, A., Remy, E., Lazar, A., Speich, S., Goes, M., Dorrington, T., Johns, W. E., Moum, J. N., Robinson, C., Perruches, C., de Souza, R. B., Gaye, A. T., Lopez-Paragess, J., Monerie, P. A., Castellanos, P., Benson, N. U., Hounkonnou, M. N., Duha, J. T., Laxenairess, R., and Reul, N.: The Tropical Atlantic Observing System, Front. Mar. Sci., 6, 206, https://doi.org/10.3389/fmars.2019.00206, 2019.

Fu, Y., Brandt, P., Tuchen, F. P., Lübbecke, J. F., and Wang, C. Z.: Representation of the mean Atlantic subtropical cells in CMIP6 models, J. Geophys. Res.-Oceans, 127, e2021JC018191, https://doi.org/10.1029/2021JC018191, 2022.

Gammelsrød, T., Bartholomae, C. H., Boyer, D. C., Filipe, V. L. L., and O'Toole, M. J.: Intrusion of warm surface water along the Angolan-Namibian coast in February–March 1995: The 1995 Benguela Niño, S. Afr. J. Marine Sci., 19, 41–56, https://doi.org/10.2989/025776198784126719, 1998.

Garzoli, S. L. and Katz, E. J.: The Forced Annual Reversal of the Atlantic North Equatorial Countercurrent, J. Phys. Oceanogr., 13, 2082–2090, https://doi.org/10.1175/1520-0485(1983)013<2082:Tfarot>2.0.Co;2, 1983.

Giordani, H. and Caniaux, G.: Diagnosing vertical motion in the Equatorial Atlantic, Ocean Dynam., 61, 1995–2018, https://doi.org/10.1007/s10236-011-0467-7, 2011.

Grodsky, S. A., Carton, J. A., and McClain, C. R.: Variability of upwelling and chlorophyll in the equatorial Atlantic, Geophys. Res. Lett., 35, L03610, https://doi.org/10.1029/2007gl032466, 2008.

Hall, R. A., Huthnance, J. M., and Williams, R. G.: Internal wave reflection on shelf slopes with depth-varying stratification, J. Phys. Oceanogr., 43, 248–258, https://doi.org/10.1175/Jpo-D-11-0192.1, 2013.

Hammond, M. L., Beaulieu, C., Henson, S. A., and Sahu, S. K.: Regional surface chlorophyll trends and uncertainties in the global ocean, Sci. Rep., 10, 15273, https://doi.org/10.1038/s41598-020-72073-9, 2020.

Han, W. Q., McCreary, J. P., Masumoto, Y., Vialard, J., and Duncan, B.: Basin Resonances in the Equatorial Indian Ocean, J. Phys. Oceanogr., 41, 1252–1270, https://doi.org/10.1175/2011jpo4591.1, 2011.

Hardman-Mountford, N. J. and McGlade, J. M.: Seasonal and interannual variability of oceanographic processes in the Gulf of Guinea: an investigation using AVHRR sea sur-

face temperature data, Int. J. Remote Sens., 24, 3247–3268, https://doi.org/10.1080/0143116021000021297, 2003.

Herbert, G., Bourlès, B., Penven, P., and Grelet, J.: New insights on the upper layer circulation north of the Gulf of Guinea, J. Geophys. Res.-Oceans, 121, 6793–6815, https://doi.org/10.1002/2016jc011959, 2016.

Herbland, A. and Voituriez, B.: Hydrological Structure-Analysis for Estimating the Primary Production in the Tropical Atlantic Ocean, J. Mar. Res., 37, 87–101, 1979.

Heukamp, F. O., Brandt, P., Dengler, M., Tuchen, F. P., McPhaden, M. J., and Moum, J. N.: Tropical instability waves and wind-forced cross-equatorial flow in the central Atlantic Ocean, Geophys. Res. Lett., 49, e2022GL099325, https://doi.org/10.1029/2022GL099325, 2022.

Hisard, P.: El-Niño response of the eastern Tropical Atlantic, Oceanol. Acta, 3, 69–78, 1980.

Hormann, V. and Brandt, P.: Upper equatorial Atlantic variability during 2002 and 2005 associated with equatorial Kelvin waves, J. Geophys. Res.-Oceans, 114, C03007, https://doi.org/10.1029/2008jc005101, 2009.

Hughes, C. W., Fukumori, I., Griffies, S. M., Huthnance, J. M., Minobe, S., Spence, P., Thompson, K. R., and Wise, A.: Sea Level and the Role of Coastal Trapped Waves in Mediating the Influence of the Open Ocean on the Coast, Surv. Geophys., 40, 1467–1492, https://doi.org/10.1007/s10712-019-09535-x, 2019.

Hummels, R., Dengler, M., and Bourlès, B.: Seasonal and regional variability of upper ocean diapycnal heat flux in the Atlantic cold tongue, Prog. Oceanogr., 111, 52–74, https://doi.org/10.1016/j.pocean.2012.11.001, 2013.

Hummels, R., Dengler, M., Brandt, P., and Schlundt, M.: Diapycnal heat flux and mixed layer heat budget within the Atlantic Cold Tongue, Clim. Dynam., 43, 3179–3199, https://doi.org/10.1007/s00382-014-2339-6, 2014.

Hutchings, L., van der Lingen, C. D., Shannon, L. J., Crawford, R. J. M., Verheye, H. M. S., Bartholomae, C. H., van der Plas, A. K., Louw, D., Kreiner, A., Ostrowski, M., Fidel, Q., Barlow, R. G., Lamont, T., Coetzee, J., Shillington, F., Veitch, J., Currie, J. C., and Monteiro, P. M. S.: The Benguela Current: An ecosystem of four components, Prog. Oceanogr., 83, 15–32, https://doi.org/10.1016/j.pocean.2009.07.046, 2009.

Illig, S., Dewitte, B., Ayoub, N., du Penhoat, Y., Reverdin, G., De Mey, P., Bonjean, F., and Lagerloef, G. S. E.: Interannual long equatorial waves in the tropical Atlantic from a high-resolution ocean general circulation model experiment in 1981–2000, J. Geophys. Res.-Oceans, 109, C02022, https://doi.org/10.1029/2003jc001771, 2004.

Illig, S., Bachèlery, M. L., and Cadier, E.: Subseasonal coastal-trapped wave propagations in the southeastern Pacific and Atlantic oceans: 2. Wave characteristics and connection with the equatorial variability, J. Geophys. Res.-Oceans, 123, 3942–3961, https://doi.org/10.1029/2017jc013540, 2018a.

Illig, S., Cadier, E., Bachèlery, M. L., and Kersale, M.: Subseasonal coastal-trapped wave propagations in the southeastern Pacific and Atlantic oceans: 1. A new approach to estimate wave amplitude, J. Geophys. Res.-Oceans, 123, 3915–3941, https://doi.org/10.1029/2017jc013539, 2018b.

Imbol Koungue, R. A. and Brandt, P.: Impact of intraseasonal waves on Angolan warm and cold events, J. Geophys. Res.-Oceans, 126, e2020JC017088, https://doi.org/10.1029/2020JC017088, 2021.

Imbol Koungue, R. A., Illig, S., and Rouault, M.: Role of interannual Kelvin wave propagations in the equatorial Atlantic on the Angola Benguela Current system, J. Geophys. Res.-Oceans, 122, 4685–4703, https://doi.org/10.1002/2016jc012463, 2017.

Imbol Koungue, R. A., Rouault, M., Illig, S., Brandt, P., and Jouanno, J.: Benguela Niños and Benguela Niñas in Forced Ocean Simulation From 1958 to 2015, J. Geophys. Res.-Oceans, 124, 5923–5951, https://doi.org/10.1029/2019jc015013, 2019.

Imbol Koungue, R. A., Brandt, P., Lübbecke, J. F., Prigent, A., Sena Martins, M., and Rodrigues, R. R.: The 2019 Benguela Niño, Front. Mar. Sci., 8, 800103, https://doi.org/10.3389/fmars.2021.800103, 2021.

Ingham, M. C.: Coastal upwelling in northwestern Gulf of Guinea, B. Mar. Sci., 20, 1–34, 1970.

Johns, W. E., Brandt, P., Bourlès, B., Tantet, A., Papapostolou, A., and Houk, A.: Zonal structure and seasonal variability of the Atlantic Equatorial Undercurrent, Clim. Dynam., 43, 3047–3069, https://doi.org/10.1007/s00382-014-2136-2, 2014.

Jouanno, J., Marin, F., du Penhoat, Y., Molines, J. M., and Sheinbaum, J.: Seasonal modes of surface cooling in the Gulf of Guinea, J. Phys. Oceanogr., 41, 1408–1416, https://doi.org/10.1175/Jpo-D-11-031.1, 2011a.

Jouanno, J., Marin, F., du Penhoat, Y., Sheinbaum, J., and Molines, J. M.: Seasonal heat balance in the upper 100 m of the equatorial Atlantic Ocean, J. Geophys. Res.-Oceans, 116, C09003, https://doi.org/10.1029/2010jc006912, 2011b.

Jouanno, J., Marin, F., du Penhoat, Y., and Molines, J. M.: Intraseasonal modulation of the surface cooling in the Gulf of Guinea, J. Phys. Oceanogr., 43, 382–401, https://doi.org/10.1175/Jpo-D-12-053.1, 2013.

Jouanno, J., Hernandez, O., and Sanchez-Gomez, E.: Equatorial Atlantic interannual variability and its relation to dynamic and thermodynamic processes, Earth Syst. Dynam., 8, 1061–1069, https://doi.org/10.5194/esd-8-1061-2017, 2017.

Kämpf, J.: On the magnitude of upwelling fluxes in shelf-break canyons, Cont. Shelf Res., 27, 2211–2223, https://doi.org/10.1016/j.csr.2007.05.010, 2007.

Katz, E. J. and Garzoli, S.: Response of the western Equatorial Atlantic Ocean to an annual wind cycle, J. Mar. Res., 40, 307–327, 1982.

Keenlyside, N. S. and Latif, M.: Understanding equatorial Atlantic interannual variability, J. Climate, 20, 131–142, https://doi.org/10.1175/Jcli3992.1, 2007.

Kiko, R., Biastoch, A., Brandt, P., Cravatte, S., Hauss, H., Hummels, R., Kriest, I., Marin, F., McDonnell, A. M. P., Oschlies, A., Picheral, M., Schwarzkopf, F. U., Thurnherr, A. M., and Stemmann, L.: Biological and physical influences on marine snowfall at the equator, Nat. Geosci., 10, 852–858, https://doi.org/10.1038/Ngeo3042, 2017.

Knight, J. R., Folland, C. K., and Scaife, A. A.: Climate impacts of the Atlantic Multidecadal Oscillation, Geophys. Res. Lett., 33, L17706, https://doi.org/10.1029/2006gl026242, 2006.

Kolodziejczyk, N., Marin, F., Bourlès, B., Gouriou, Y., and Berger, H.: Seasonal variability of the equatorial undercurrent termination and associated salinity maximum in the Gulf of Guinea, Clim. Dynam., 43, 3025–3046, https://doi.org/10.1007/s00382-014-2107-7, 2014.

Koné, V., Lett, C., Penven, P., Bourles, B., and Djakouré, S.: A biophysical model of S. aurita early life history in the northern Gulf of Guinea, Prog. Oceanogr., 151, 83–96, https://doi.org/10.1016/j.pocean.2016.10.008, 2017.

Kopte, R., Brandt, P., Dengler, M., Tchipalanga, P. C. M., Macueria, M., and Ostrowski, M.: The Angola Current: Flow and hydrographic characteristics as observed at 11° S, J. Geophys. Res.-Oceans, 122, 1177–1189, https://doi.org/10.1002/2016jc012374, 2017.

Kopte, R., Brandt, P., Claus, M., Greatbatch, R. J., and Dengler, M.: Role of equatorial basin-mode resonance for the seasonal variability of the Angola Current at 11° S, J. Phys. Oceanogr., 48, 261–281, https://doi.org/10.1175/Jpo-D-17-0111.1, 2018.

Körner, M., Brandt, P., and Dengler, M.: Seasonal cycle of sea surface temperature in the tropical Angolan Upwelling System, Ocean Sci., 19, 121–139, https://doi.org/10.5194/os-19-121-2023, 2023.

Lamb, K. G.: Internal wave breaking and dissipation mechanisms on the continental slope/shelf, Annu. Rev. Fluid Mech., 46, 231–254, https://doi.org/10.1146/annurev-fluid-011212-140701, 2014.

Longhurst, A.: Seasonal cooling and blooming in tropical oceans, Deep-Sea Res. Pt. I, 40, 2145–2165, https://doi.org/10.1016/0967-0637(93)90095-K, 1993.

Loukos, H. and Memery, L.: Simulation of the nitrate seasonal cycle in the equatorial Atlantic Ocean during 1983 and 1984, J. Geophys. Res.-Oceans, 104, 15549–15573, https://doi.org/10.1029/1999jc900084, 1999.

Lübbecke, J. F., Rodriguez-Fonseca, B., Richter, I., Martin-Rey, M., Losada, T., Polo, I., and Keenlyside, N. S.: Equatorial Atlantic variability – Modes, mechanisms, and global teleconnections, WIREs Clim. Change, 9, e527, https://doi.org/10.1002/wcc.527, 2018.

Lübbecke, J. F., Brandt, P., Dengler, M., Kopte, R., Ludke, J., Richter, I., Martins, M. S., and Tchipalanga, P. C. M.: Causes and evolution of the southeastern tropical Atlantic warm event in early 2016, Clim. Dynam., 53, 261–274, https://doi.org/10.1007/s00382-018-4582-8, 2019.

Mao, Z. X., Mao, Z. H., Jamet, C., Linderman, M., Wang, Y. T., and Chen, X. Y.: Seasonal Cycles of Phytoplankton Expressed by Sine Equations Using the Daily Climatology from Satellite-Retrieved Chlorophyll-*a* Concentration (1997–2019) Over Global Ocean, Remote Sens.-Basel, 12, 2662, https://doi.org/10.3390/rs12162662, 2020.

Marchal, E. and Picaut, J.: Répartition et abondance évaluées par échointégration des poissons du plateau ivoiro-ghanéen en relation avec les upwellings locaux, J. Rech. Océanogr., 2, 39–58, 1977.

Marchesiello, P. and Estrade, P.: Upwelling limitation by onshore geostrophic flow, J. Mar. Res., 68, 37–62, https://doi.org/10.1357/002224010793079004, 2010.

Martins, M. S. and Stammer, D.: Interannual variability of the Congo River plume-induced sea surface salinity, Remote Sens.-Basel, 14, 1013, https://doi.org/10.3390/rs14041013, 2022.

Menkes, C. E., Kennan, S. C., Flament, P., Dandonneau, Y., Masson, S., Biessy, B., Marchal, E., Eldin, G., Grelet, J., Montel, Y., Morliere, A., Lebourges-Dhaussy, A., Moulin, C., Champalbert, G., and Herbland, A.: A whirling ecosystem in the equatorial Atlantic, Geophys. Res. Lett., 29, 1553, https://doi.org/10.1029/2001gl014576, 2002.

Merle, J.: Seasonal Heat-Budget in the Equatorial Atlantic-Ocean, J. Phys. Oceanogr., 10, 464–469, https://doi.org/10.1175/1520-0485(1980)010<0464:Shbite>2.0.Co;2, 1980.

Microwave OI SST and CCMP wind data: Research-Quality Geophysical Products from Satellite Microwave Sensors, Microwave Climate Data Center (MCDC), Remote Sensing Systems (RSS), https://www.remss.com, last access: 11 April 2023.

Monger, B., McClain, C., and Murtugudde, R.: Seasonal phytoplankton dynamics in the eastern tropical Atlantic, J. Geophys. Res.-Oceans, 102, 12389–12411, https://doi.org/10.1029/96jc03982, 1997.

Moore, D., Hisard, P., Mccreary, J., Merle, J., Obrien, J., Picaut, J., Verstraete, J. M., and Wunsch, C.: Equatorial adjustment in the eastern Atlantic, Geophys. Res. Lett., 5, 637–640, https://doi.org/10.1029/GL005i008p00637, 1978.

Moore, J. K., Doney, S. C., and Lindsay, K.: Upper ocean ecosystem dynamics and iron cycling in a global three-dimensional model, Global Biogeochem. Cy., 18, Gb4028, https://doi.org/10.1029/2004gb002220, 2004.

Mosquera-Vasquez, K., Dewitte, B., and Illig, S.: The Central Pacific El Nino intraseasonal Kelvin wave, J. Geophys. Res.-Oceans, 119, 6605–6621, https://doi.org/10.1002/2014jc010044, 2014.

Moum, J. N., Lien, R. C., Perlin, A., Nash, J. D., Gregg, M. C., and Wiles, P. J.: Sea surface cooling at the Equator by subsurface mixing in tropical instability waves, Nat. Geosci., 2, 761–765, https://doi.org/10.1038/Ngeo657, 2009.

Moum, J. N., Hughes, K. G., Shroyer, E. L., Smyth, W. D., Cherian, D., Warner, S. J., Bourles, B., Brandt, P., and Dengler, M.: Deep Cycle Turbulence in Atlantic and Pacific Cold Tongues, Geophys. Res. Lett., 49, e2021GL097345, https://doi.org/10.1029/2021GL097345, 2022.

Nnamchi, H. C., Li, J. P., Kucharski, F., Kang, I. S., Keenlyside, N. S., Chang, P., and Farneti, R.: Thermodynamic controls of the Atlantic Nino, Nat. Commun., 6, 8895, https://doi.org/10.1038/ncomms9895, 2015.

Nyadjro, E. S., Foli, B. A. K., Agyekum, K. A., Wiafe, G., and Tsei, S.: Seasonal Variability of Sea Surface Salinity in the NW Gulf of Guinea from SMAP Satellite, Remote Sens. Earth Syst. Sci., 5, 83–94, https://doi.org/10.1007/s41976-021-00061-2, 2022.

Okumura, Y. and Xie, S. P.: Some overlooked features of tropical Atlantic climate leading to a new Nino-like phenomenon, J. Climate, 19, 5859–5874, https://doi.org/10.1175/Jcli3928.1, 2006.

Oschlies, A., Brandt, P., Stramma, L., and Schmidtko, S.: Drivers and mechanisms of ocean deoxygenation, Nat. Geosci., 11, 467–473, https://doi.org/10.1038/s41561-018-0152-2, 2018.

Ostrowski, M., da Silva, J. C. B., and Bazik-Sangolay, B.: The response of sound scatterers to El Niño- and La Niña-like oceanographic regimes in the southeastern Atlantic, ICES J. Mar. Sci., 66, 1063–1072, https://doi.org/10.1093/icesjms/fsp102, 2009.

Perez, R. C., Hormann, V., Lumpkin, R., Brandt, P., Johns, W. E., Hernandez, F., Schmid, C., and Bourlès, B.: Mean meridional currents in the central and eastern equatorial Atlantic, Clim. Dynam., 43, 2943–2962, https://doi.org/10.1007/s00382-013-1968-5, 2014.

Perlin, A., Moum, J. N., and Klymak, J. M.: Response of the bottom boundary layer over a sloping shelf to variations

in alongshore wind, J. Geophys. Res.-Oceans, 110, C10S09, https://doi.org/10.1029/2004jc002500, 2005.

Philander, S. G. H.: Upwelling in the Gulf of Guinea, J. Mar. Res., 37, 23–33, 1979.

Philander, S. G. H. and Pacanowski, R. C.: Response of equatorial oceans to periodic forcing, J. Geophys. Res.-Oceans, 86, 1903–1916, https://doi.org/10.1029/Jc086ic03p01903, 1981.

Philander, S. G. H. and Pacanowski, R. C.: A model of the seasonal cycle in the tropical Atlantic-Ocean, J. Geophys. Res.-Oceans, 91, 14192–14206, https://doi.org/10.1029/JC091iC12p14192, 1986.

Picaut, J.: Propagation of the Seasonal Upwelling in the Eastern Equatorial Atlantic, J. Phys. Oceanogr., 13, 18–37, https://doi.org/10.1175/1520-0485(1983)013<0018:Potsui>2.0.Co;2, 1983.

Polo, I., Lazar, A., Rodriguez-Fonseca, B., and Arnault, S.: Oceanic Kelvin waves and tropical Atlantic intraseasonal variability: 1. Kelvin wave characterization, J. Geophys. Res.-Oceans, 113, C07009, https://doi.org/10.1029/2007jc004495, 2008.

Prigent, A., Imbol Koungue, R. A., Lübbecke, J. F., Brandt, P., and Latif, M.: Origin of weakened interannual sea surface temperature variability in the southeastern tropical Atlantic Ocean, Geophys. Res. Lett., 47, e2020GL089348, https://doi.org/10.1029/2020GL089348, 2020a.

Prigent, A., Lübbecke, J. F., Bayr, T., Latif, M., and Wengel, C.: Weakened SST variability in the tropical Atlantic Ocean since 2000, Clim. Dynam., 54, 2731–2744, https://doi.org/10.1007/s00382-020-05138-0, 2020b.

Rabe, B., Schott, F. A., and Köhl, A.: Mean circulation and variability of the tropical Atlantic during 1952–2001 in the GECCO assimilation fields, J. Phys. Oceanogr., 38, 177–192, https://doi.org/10.1175/2007jpo3541.1, 2008.

Radenac, M.-H., Jouanno, J., Tchamabi, C. C., Awo, M., Bourlès, B., Arnault, S., and Aumont, O.: Physical drivers of the nitrate seasonal variability in the Atlantic cold tongue, Biogeosciences, 17, 529–545, https://doi.org/10.5194/bg-17-529-2020, 2020.

Richter, I., Behera, S. K., Masumoto, Y., Taguchi, B., Komori, N., and Yamagata, T.: On the triggering of Benguela Niños: Remote equatorial versus local influences, Geophys. Res. Lett., 37, L20604, https://doi.org/10.1029/2010gl044461, 2010.

Roch, M., Brandt, P., Schmidtko, S., Vaz Velho, F., and Ostrowski, M.: Southeastern tropical Atlantic changing from subtropical to tropical conditions, Front. Mar. Sci., 8, 748383, https://doi.org/10.3389/fmars.2021.748383, 2021.

Rossi, V., Feng, M., Pattiaratchi, C., Roughan, M., and Waite, A. M.: On the factors influencing the development of sporadic upwelling in the Leeuwin Current system, J. Geophys. Res.-Oceans, 118, 3608–3621, https://doi.org/10.1002/jgrc.20242, 2013.

Rouault, M.: Bi-annual intrusion of tropical water in the northern Benguela upwelling, Geophys. Res. Lett., 39, L12606, https://doi.org/10.1029/2012gl052099, 2012.

Rouault, M., Illig, S., Bartholomae, C., Reason, C. J. C., and Bentamy, A.: Propagation and origin of warm anomalies in the Angola Benguela upwelling system in 2001, J. Marine Syst., 68, 473–488, https://doi.org/10.1016/j.jmarsys.2006.11.010, 2007.

Rouault, M., Illig, S., Lübbecke, J. F., and Imbol Koungue, R. A.: Origin, development and demise of the 2010–2011 Benguela Niño, J. Marine Syst., 188, 39–48, https://doi.org/10.1016/j.jmarsys.2017.07.007, 2018.

Ruiz-Barradas, A., Carton, J. A., and Nigam, S.: Structure of interannual-to-decadal climate variability in the tropical Atlantic sector, J. Climate, 13, 3285–3297, https://doi.org/10.1175/1520-0442(2000)013<3285:Soitdc>2.0.Co;2, 2000.

Sallee, J. B., Pellichero, V., Akhoudas, C., Pauthenet, E., Vignes, L., Schmidtko, S., Garabato, A. N., Sutherland, P., and Kuusela, M.: Summertime increases in upper-ocean stratification and mixed-layer depth, Nature, 591, 592–598, https://doi.org/10.1038/s41586-021-03303-x, 2021.

Schafstall, J., Dengler, M., Brandt, P., and Bange, H.: Tidal-induced mixing and diapycnal nutrient fluxes in the Mauritanian upwelling region, J. Geophys. Res.-Oceans, 115, C10014, https://doi.org/10.1029/2009jc005940, 2010.

Schott, F. A., Fischer, J., and Stramma, L.: Transports and pathways of the upper-layer circulation in the western tropical Atlantic, J. Phys. Oceanogr., 28, 1904–1928, https://doi.org/10.1175/1520-0485(1998)028<1904:TAPOTU>2.0.CO;2, 1998.

Schott, F. A., McCreary, J. P., and Johnson, G. C.: Shallow overturning circulations of the tropical-subtropical oceans, in: Earth Climate: The Ocean-Atmosphere Interaction, edited by: Wang, C., Xie, S.-P., and Carton, J. A., Geophysical Monograph 147, American Geophysical Union, Washington, DC, 261–304, https://doi.org/10.1029/147GM15, 2004.

Servain, J., Picaut, J., and Merle, J.: Evidence of Remote Forcing in the Equatorial Atlantic-Ocean, J Phys Oceanogr, 12, 457-463, https://doi.org/10.1175/1520-0485(1982)012<0457:Eorfit>2.0.Co;2, 1982.

Shannon, L. V., Boyd, A. J., Brundrit, G. B., and Taunton-Clark, J.: On the Existence of an El-Niño-Type Phenomenon in the Benguela System, J. Mar. Res., 44, 495–520, https://doi.org/10.1357/002224086788403105, 1986.

Sherman, J., Subramaniam, A., Gorbunov, M. Y., Fernandez-Carrera, A., Kiko, R., Brandt, P., and Falkowski, P. G.: The photophysiological response of nitrogen-limited phytoplankton to episodic nitrogen supply associated with Tropical Instability Waves in the equatorial Atlantic, Front. Mar. Sci., 8, 814663, https://doi.org/10.3389/fmars.2021.814663, 2022.

Siegfried, L., Schmidt, M., Mohrholz, V., Pogrzeba, H., Nardini, P., Böttinger, M., and Scheuermann, G.: The tropical-subtropical coupling in the Southeast Atlantic from the perspective of the northern Benguela upwelling system, Plos One, 14, e0210083, https://doi.org/10.1371/journal.pone.0210083, 2019.

Sohou, Z., Koné, V., Da-Allada, Y. C., Djakouré, S., Bourlès, B., Racape, V., Degbe, G., and Adje, C.: Seasonal and inter-annual ONSET Sea Surface Temperature variability along the northern coast of the Gulf of Guinea, Reg. Stud. Mar. Sci., 35, 101129, https://doi.org/10.1016/j.rsma.2020.101129, 2020.

Sowman, M. and Cardoso, P.: Small-scale fisheries and food security strategies in countries in the Benguela Current Large Marine Ecosystem (BCLME) region: Angola, Namibia and South Africa, Mar. Policy, 34, 1163–1170, https://doi.org/10.1016/j.marpol.2010.03.016, 2010.

Tchipalanga, P., Dengler, M., Brandt, P., Kopte, R., Macueria, M., Coelho, P., Ostrowski, M., and Keenlyside, N. S.: Eastern Boundary Circulation and Hydrography Off Angola: Building Angolan Oceanographic Capacities, B. Am. Meteorol. Soc., 99, 1589–1605, https://doi.org/10.1175/Bams-D-17-0197.1, 2018a.

Tchipalanga, P. C. M., Ostrowski, M., and Dengler, M.: Physical oceanography (CTD) during Fridtjof Nansen cruise FN1998409, PANGAEA [data set], https://doi.org/10.1594/PANGAEA.887163, 2018b.

Thomsen, S., Kanzow, T., Krahmann, G., Greatbatch, R. J., Dengler, M., and Lavik, G.: The formation of a subsurface anticyclonic eddy in the Peru-Chile Undercurrent and its impact on the near-coastal salinity, oxygen, and nutrient distributions, J. Geophys. Res.-Oceans, 121, 476–501, https://doi.org/10.1002/2015jc010878, 2016.

Thomsen, S., Capet, X., and Echevin, V.: Competition between Baroclinic Instability and Ekman Transport under Varying Buoyancy Forcings in Upwelling Systems: An Idealized Analog to the Southern Ocean, J. Phys. Oceanogr., 51, 3347–3364, https://doi.org/10.1175/Jpo-D-20-0294.1, 2021.

Tokinaga, H. and Xie, S. P.: Weakening of the equatorial Atlantic cold tongue over the past six decades, Nat. Geosci., 4, 222–226, https://doi.org/10.1038/Ngeo1078, 2011.

Toualy, E., Kouacou, B., and Aman, A.: Influence of Wind and Surface Buoyancy Flux on the Variability of the Oceanic Mixed Layer Depth in the Northern Gulf of Guinea Coastal Upwelling, Thalassas, 38, 599–608, https://doi.org/10.1007/s41208-021-00358-5, 2022.

Tuchen, F. P., Lübbecke, J. F., Schmidtko, S., Hummels, R., and Böning, C. W.: The Atlantic Subtropical Cells Inferred from Observations, J. Geophys. Res.-Oceans, 124, 7591–7605, https://doi.org/10.1029/2019jc015396, 2019.

Tuchen, F. P., Lübbecke, J. F., Brandt, P., and Fu, Y.: Observed transport variability of the Atlantic Subtropical Cells and their connection to tropical sea surface temperature variability, J. Geophys. Res.-Oceans, 125, e2020JC016592, https://doi.org/10.1029/2020JC016592, 2020.

Tuchen, F. P., Brandt, P., Lübbecke, J. F., and Hummels, R.: Transports and pathways of the tropical AMOC return flow from Argo data and shipboard velocity measurements, J. Geophys. Res.-Oceans, 127, e2021JC018115, https://doi.org/10.1029/2021JC018115, 2022a.

Tuchen, F. P., Perez, R. C., Foltz, G. R., Brandt, P., and Lumpkin, R.: Multidecadal intensification of Atlantic tropical instability waves, Geophys. Res. Lett., 49, e2022GL101073, https://doi.org/10.1029/2022GL101073, 2022b.

Voituriez, B., Herbland, A., and Le Borgne, R.: L'upwelling eìquatorial de l'Atlantique Est pendant l'Expérience Météorologique Mondiale (PEMG), Oceanol. Acta, 5, 301–314, 1982.

Wade, M., Caniaux, G., and du Penhoat, Y.: Variability of the mixed layer heat budget in the eastern equatorial Atlantic during 2005–2007 as inferred using Argo floats, J. Geophys. Res.-Oceans, 116, C08006, https://doi.org/10.1029/2010jc006683, 2011.

Wang, D. W., Gouhier, T. C., Menge, B. A., and Ganguly, A. R.: Intensification and spatial homogenization of coastal upwelling under climate change, Nature, 518, 390–394, https://doi.org/10.1038/nature14235, 2015.

Warner, S. J., Holmes, R. M., Hawkins, E. H. M., Hoecker-Martinez, M. S., Savage, A. C., and Moum, J. N.: Buoyant gravity currents released from Tropical Instability Waves, J. Phys. Oceanogr., 48, 361–382, https://doi.org/10.1175/Jpo-D-17-0144.1, 2018.

Weingartner, T. J. and Weisberg, R. H.: On the Annual Cycle of Equatorial Upwelling in the Central Atlantic-Ocean, J. Phys. Oceanogr., 21, 68–82, https://doi.org/10.1175/1520-0485(1991)021<0068:Otacoe>2.0.Co;2, 1991.

Wiafe, G. and Nyadjro, E. S.: Satellite Observations of Upwelling in the Gulf of Guinea, IEEE Geosci. Remote S., 12, 1066–1070, https://doi.org/10.1109/Lgrs.2014.2379474, 2015.

Yang, H., Lohmann, G., Krebs-Kanzow, U., Ionita, M., Shi, X. X., Sidorenko, D., Gong, X., Chen, X. E., and Gowan, E. J.: Poleward Shift of the Major Ocean Gyres Detected in a Warming Climate, Geophys. Res. Lett., 47, e2019GL085868, https://doi.org/10.1029/2019GL085868, 2020.

Yang, Y., Wu, L. X., Cai, W. J., Jia, F., Ng, B., Wang, G. J., and Geng, T.: Suppressed Atlantic Nino/Nina variability under greenhouse warming, Nat. Clim. Change, 12, 814–821, https://doi.org/10.1038/s41558-022-01444-z, 2022.

Zeng, Z., Brandt, P., Lamb, K. G., Greatbatch, R. J., Dengler, M., Claus, M., and Chen, X.: Three-dimensional numerical simulations of internal tides in the Angolan upwelling region, J. Geophys. Res.-Oceans, 126, e2020JC016460, https://doi.org/10.1029/2020JC016460, 2021.